Fructose-Induced mTORC1 Activation Promotes Pancreatic Cancer Progression through Inhibition of Autophagy

Yanfen Cui[1], Jianfei Tian[1], Zhaosong Wang[2], Hui Guo[1], He Zhang[1], Zhiyong Wang[1], Hui Liu[1], Weijie Song[2], Liming Liu[1], Ruinan Tian[1], Xiaoyan Zuo[1], Sixin Ren[1], Ruifang Niu[1], and Fei Zhang[1]

ABSTRACT

Excessive fructose intake is associated with the occurrence, progression, and poor prognosis of various tumors. A better understanding of the mechanisms underlying the functions of fructose in cancer could facilitate the development of better treatment and prevention strategies. In this study, we investigated the functional association between fructose utilization and pancreatic ductal adenocarcinoma (PDAC) progression. Fructose could be taken up and metabolized by PDAC cells and provided an adaptive survival mechanism for PDAC cells under glucose-deficient conditions. GLUT5-mediated fructose metabolism maintained the survival, proliferation, and invasion capacities of PDAC cells *in vivo* and *in vitro*. Fructose metabolism not only provided ATP and biomass to PDAC cells but also conferred metabolic plasticity to the cells, making them more adaptable to the tumor microenvironment. Mechanistically, fructose activated the AMP-activated protein kinase (AMPK)–mTORC1 signaling pathway to inhibit glucose deficiency-induced autophagic cell death. Moreover, the fructose-specific transporter GLUT5 was highly expressed in PDAC tissues and was an independent marker of disease progression in patients with PDAC. These findings provide mechanistic insights into the role of fructose in promoting PDAC progression and offer potential strategies for targeting metabolism to treat PDAC.

Significance: Fructose activates AMPK–mTORC1 signaling to inhibit autophagy-mediated cell death in pancreatic cancer cells caused by glucose deficiency, facilitating metabolic adaptation to the tumor microenvironment and supporting tumor growth.

Introduction

Pancreatic ductal adenocarcinoma (PDAC) accounts for approximately 90% of all pancreatic cancers and is one of the most aggressive solid tumors (1). Evidence suggests that the development of PDAC may be related to smoking, unhealthy diet, environmental pollution, and genetic factors (2). Epidemiological studies have found that the incidence of pancreatic cancer is significantly higher in patients with diabetes and chronic pancreatitis than in the general population (3, 4). Despite recent advances in diagnosis and therapy, the overall cumulative 5-year survival rate is less than 9% due to its early metastasis and chemoresistance (5), making the treatment of patients with PDAC extremely challenging. Validated prevention strategies, early diagnosis, and effective systemic therapy are urgently needed to reduce the incidence of PDAC, suppress its malignant progression, and improve patient survival. Therefore, unraveling the mechanisms leading to PDAC initiation and progression will help to identify new markers for the diagnosis of this malignancy as well as new therapeutic targets.

Fructose is a monosaccharide with the same chemical formula as glucose, but with a different structure. It is widely found in natural foods, such as fruits and honey, and is also a major component of high-fructose corn syrup (6). As one of the sweetest of all natural sugars, fructose is extensively used as a sweetener in processed foods, and its consumption has increased dramatically in recent decades (7). However, excessive fructose intake can promote the development and malignant progression of many kinds of tumors, and lead to poor prognosis in patients with cancer (8–18). Of all carbohydrates, high-fructose intake is most strongly associated with breast cancer (19). A systematic review and dose–response meta-analysis of several prospective studies suggested that fructose intake increases the risk of pancreatic cancer (20). In addition, women who consume high fructose are 2.1 times more likely to develop colon cancer than women on a normal diet (21), whereas men have a 27% to 37% increased incidence of colon cancer (14). Moreover, high-fructose consumption significantly reduces disease-free survival and promotes recurrence of advanced colon cancer. This effect of fructose may be related to the fact that it causes an increase in the length of intestinal villi, which has been confirmed in mouse experiments to be associated with a higher risk of colorectal cancer and greater tumor aggressiveness (22). In addition, fructose provides energy and biomass for cancer cell growth and contributes to the Warburg effect by downregulating mitochondrial respiration (23). Nevertheless, the detailed mechanisms by which fructose promotes tumorigenesis and progression remain to be elucidated.

Physiologically, fructose is passively absorbed into the intestinal lumen through the Glucose-transporter type 5 (Glut5) and metabolized mainly in the liver, kidney, and adipocytes (24). In most cases, fructose is first metabolized intracellular via KHK or HK catalysis and

[1]Public Laboratory, Tianjin Medical University Cancer Institute and Hospital, National Clinical Research Center for Cancer, Key Laboratory of Cancer Prevention and Therapy, Tianjin's Clinical Research Center for Cancer, Tianjin, China. [2]Laboratory Animal Center, Tianjin Medical University Cancer Institute and Hospital, National Clinical Research Center for Cancer, Key Laboratory of Cancer Prevention and Therapy, Tianjin's Clinical Research Center for Cancer, Tianjin, China.

Y. Cui, J. Tian, and Z. Wang contributed equally as co-authors of this article.

Corresponding Authors: Fei Zhang, Public Laboratory, Tianjin Medical University Cancer Institute and Hospital, Huan-Hu-Xi Road, He-Xi District, Tianjin 300060, China. E-mail: feizhang03@tmu.edu.cn; and Ruifang Niu, rniu@tmu.edu.cn

Cancer Res 2023;83:4063–79

doi: 10.1158/0008-5472.CAN-23-0464

then resynthesized into glucose via gluconeogenesis or integrated into lipogenic or oxidative pathways via glycolysis (Supplementary Fig. S1A; ref. 25). In fact, most normal tissues rarely express the fructose-transporter Glut5, and therefore cannot directly use and metabolize fructose (26). However, it is clear that tumor cells express Glut5 and are able to metabolize fructose (17, 27–33). As research has progressed, several studies have shown that Glut5 expression and fructose utilization in cancer tissues correlate with tumor progression and patient prognosis (17, 29, 32, 33). To date, no epidemiological investigations on the relationship between fructose intake and pancreatic cancer progression have been reported, and few experimental studies on the aforementioned relationship have been implemented. Although one research found that fructose promotes pancreatic cancer cell proliferation by increasing nucleic acid synthesis *in vivo*, this study lacked the necessary *in vivo* experiments and clinical sample testing to confirm its findings (34). Therefore, more in-depth research is needed to further investigate the role of fructose in pancreatic cancer. In this study, we report a functional association between fructose utilization and PDAC progression. We demonstrate that Glut5-mediated fructose metabolism maintains the survival, proliferation, and migration capacities of PDAC cells *in vivo* and *in vitro*. Fructose metabolism not only provides ATP and biomass to PDAC cells, but also confers metabolic plasticity to the cells, making them more adaptable to the tumor microenvironment. Mechanistically, fructose inhibits glucose deficiency–induced autophagy and promotes PDAC progression by regulating the AMPK (AMP-activated protein kinase)–mTORC1 signaling pathway. Moreover, the fructose-transporter Glut5 was highly expressed in PDAC tissues and served as an independent marker of disease progression in patients with PDAC, suggesting that targeting fructose metabolism may be a potential therapeutic strategy for PDAC.

Materials and Methods

Cell lines and cell culture

Human PDAC cell lines SW1990, SU86.86, Capan2, and BxPC3, the mouse PDAC cell line Panc02, and human embryonic kidney HEK293T cells were obtained from the ATCC. PDAC cell lines were cultured in RPMI-1640 medium (HyClone), and HEK293T cells were cultured in DMEM high-glucose medium (HyClone). All media were supplemented with 10% FBS (Gibco) and 1% penicillin and streptomycin. All cells were cultured at 37°C in an incubator with 5% CO_2. Glucose-free DMEM and dialyzed FBS (DFBS) were obtained from Gibco. Hypoxia was defined as a 1% oxygen environment. The following inhibitors were used in the experiments: Mitochondrial electron transport chain complex I inhibitor (rotenone, HY-B1756, MCE), OXPHOS (oxidative phosphorylation) uncoupler (FCCP, HY-100410, MCE), ATP synthetase inhibitor (oligomycin, HY-B1756, MCE), Glut5 inhibitor (2,5-AM, Cayman Chem), HK inhibitor (2-DG, D8375, SIGMA), KHK inhibitor (420640, SIGMA), AMPK inhibitor (Compound C, HY-13418A, MCE), and AMPK activator (AICAR, HY-13417, MCE). All cell lines were authenticated by short tandem repeat profiling and tested for *Mycoplasma* contamination.

Plasmid construction, lentivirus production, and stable cell line generation

GFP-LC3 plasmid was a gift from Prof. Binghui Li of Tianjin Medical University Cancer Institute and Hospital. The small hairpin RNAs (shRNA) were constructed into pLKO.1 plasmids to down-regulate Glut5, and the sequences were as follows: shGlut5#1: ACAAGGTGTCAGACGTATATC; shGlut5#2: GGACATTCATTGAGATCAACC. Glut5-Flag was amplified by PCR using the following primers: upper: 5′-ACCTCCATAGAAGATTCTAGAGCCACCATGGAGCAACAGGATCAGAGCA-3′, lower: 5′-TTCGAATTCGCTCAGCTCTAGATCACTTGTCGTCGTCGTCCTTATAGTCCTGTTCCGAAGTGACAGGTG-3′, and then inserted into the lentiviral vector pCDH-CMV-Puro at the Xba I–cloning site. Lentivirus was prepared by cotransfecting HEK293T cells with the lentiviral plasmids and two packaging plasmids (psPAX2 and pMD2.G) using polyethyleneimine. After 48 hours, the virus-containing supernatant was collected, and cancer cells were infected with the lentivirus for 12 hours and then selected with 1 μg/mL puromycin for 3 days. RT-PCR and Western blot were used to verify the expression level of Glut5.

Cell proliferation assay

The CCK8 assay was performed using a CCK8 kit following the manufacturer's protocol (Bimake). In brief, cells (1,000 cells/well) were seeded and incubated in 96-well plates. Then, 10 μL of CCK8 solution was added to each well and incubated for 3 hours at 37°C in an incubator. The absorbance was read at 450 nm to detect cell viability.

EdU proliferation analysis

The 5-ethynyl-2′-deoxyuridine (EdU) assay kit (Cat#C0071S, Beyotime) was used to detect cell proliferation following the manufacturer's instructions. Briefly, a total of 1×10^4 cells/well were seeded in a 96-well plate and cultured in different medium for 24 hours. The cells were then incubated with 10 μmol/L EdU for 2 hours, and fixed with 4% paraformaldehyde for 30 minutes. Subsequently, these cells were incubated with 2 mg/mL glycine for 5 minutes, and permeabilized with 0.5% Triton X-100, and reacted with Apollo solution for 30 minutes. The cells were then incubated with Hoechst solution and visualized by fluorescence microscopy. The percentage of EdU-positive cells was used to determine cell proliferative activity.

Colony formation assay

Cells (1,000 cells/well) were seeded in a 6-well plate and cultured in medium containing different sugars for 2 weeks. Then the plate was washed with PBS, fixed with methanol, stained with crystal violet staining buffer, and the number of colonies was counted under an inverted microscope, and representative images were taken.

Soft agar colony formation assay

Cells (1,000 cells/well) cultured in DMEM medium containing different sugars were suspended in low-melting agarose (GE Healthcare) to a final concentration of 0.3% on 6-well plates precoated with a solidified bottom layer made of 0.6% agarose in the same medium. After incubation for 2 weeks, the plate was washed with PBS, fixed with methanol, stained with crystal violet staining buffer, and colonies were counted using a colony counter.

Cell apoptosis analysis

Cell apoptosis assays were performed according to the instructions of the Annexin V-FITC/PI Apoptosis Detection Kit (Vazyme). Cells were seeded in 6-well plates and cultured in different media for 48 hours according to the experimental design. Then the cells were collected in 300 μL of binding buffer and stained with 5 μL of Annexin V-FITC and 5 μL of propidium iodide (PI) solution. The stained cells were analyzed using the FITC and PI channels of a flow cytometer (BD Biosciences).

Wound-healing

Cells were cultured in 6-well plates, scraped with a 200 μL pipette tip, and then washed with PBS to remove detached cells. The cells were

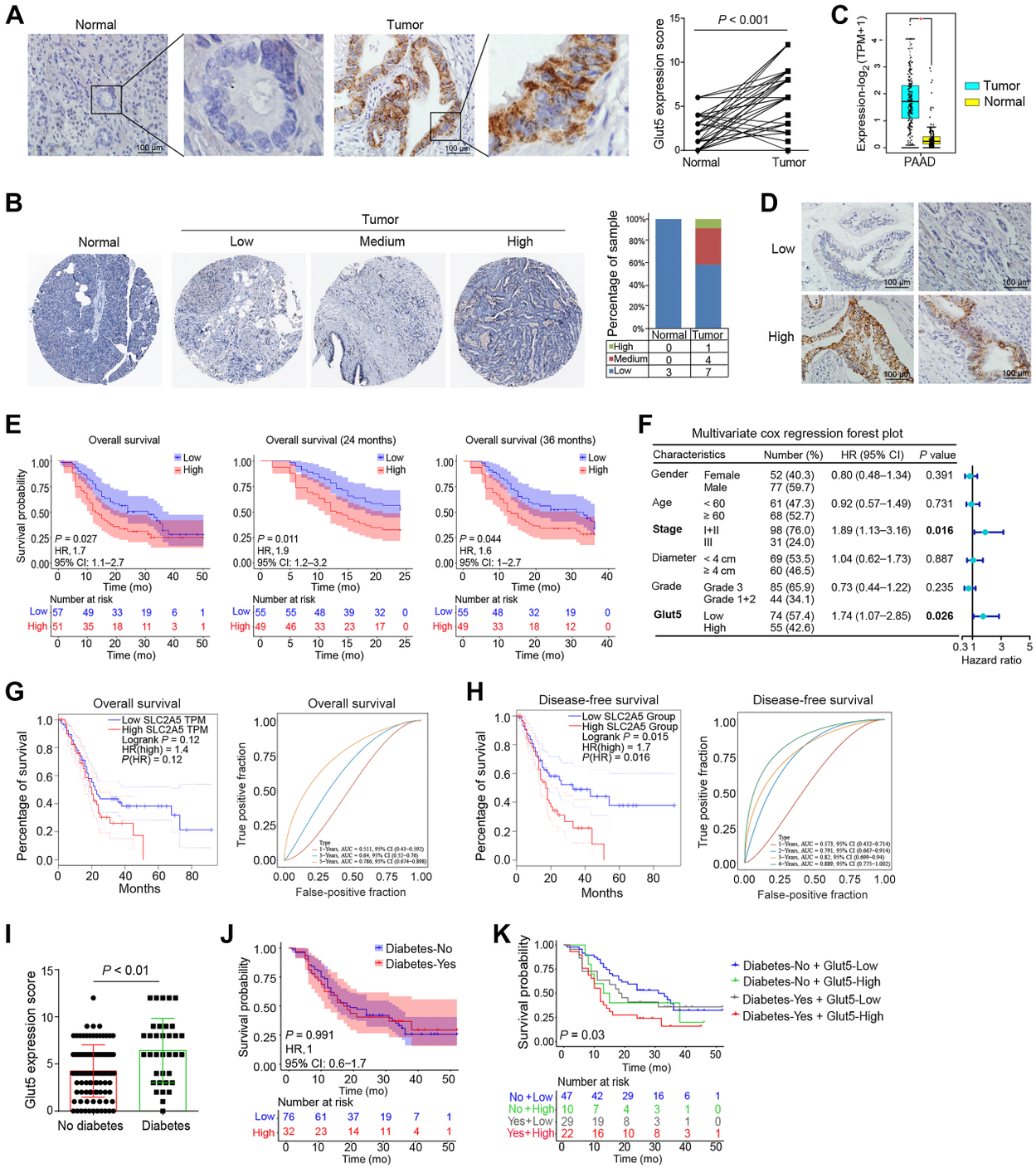

Figure 1.

Glut5 was highly expressed in PDAC tissues and associated with worse prognosis. **A,** The expression level and location of Glut5 protein in PDAC tissues (IHC, ×400) and their corresponding normal tissues were identified by IHC staining ($n = 50$). **B,** Expression levels of Glut5 protein in PDAC and normal pancreatic tissues in the Human Protein Atlas database. **C,** Expression levels of Glut5 mRNA in PDAC and normal pancreatic tissues in the TCGA database. **D,** Representative images of low and high Glut5 expressions in PDAC tissues by IHC staining (IHC, ×400; $n = 129$). **E,** Relationship between Glut5 expression levels and the prognosis of patients with PDAC. **F,** Multivariate Cox regression analysis was used to evaluate independent risk factors for prognosis of patients with PDAC. CI, confidence interval; HR, hazard ratio. **G** and **H,** Relationships between Glut5 mRNA expression levels and overall survival (**G**) and disease-free survival (**H**) of patients with PDAC in the TCGA database. **I,** Glut5 protein expression levels in PDAC tissues from diabetic and non-diabetic patients. **J,** The effect of diabetes on the survival of patients with PDAC. **K,** The effect of diabetes combined with Glut5 expression levels in tumor tissues on the prognosis of patients with PDAC. All data are expressed as mean ± SD. Analysis was performed using a paired samples *t* test (**A**) or an unpaired Student *t* test (**B** and **I**) or the Kaplan–Meier method (**E**, **J**, and **K**).

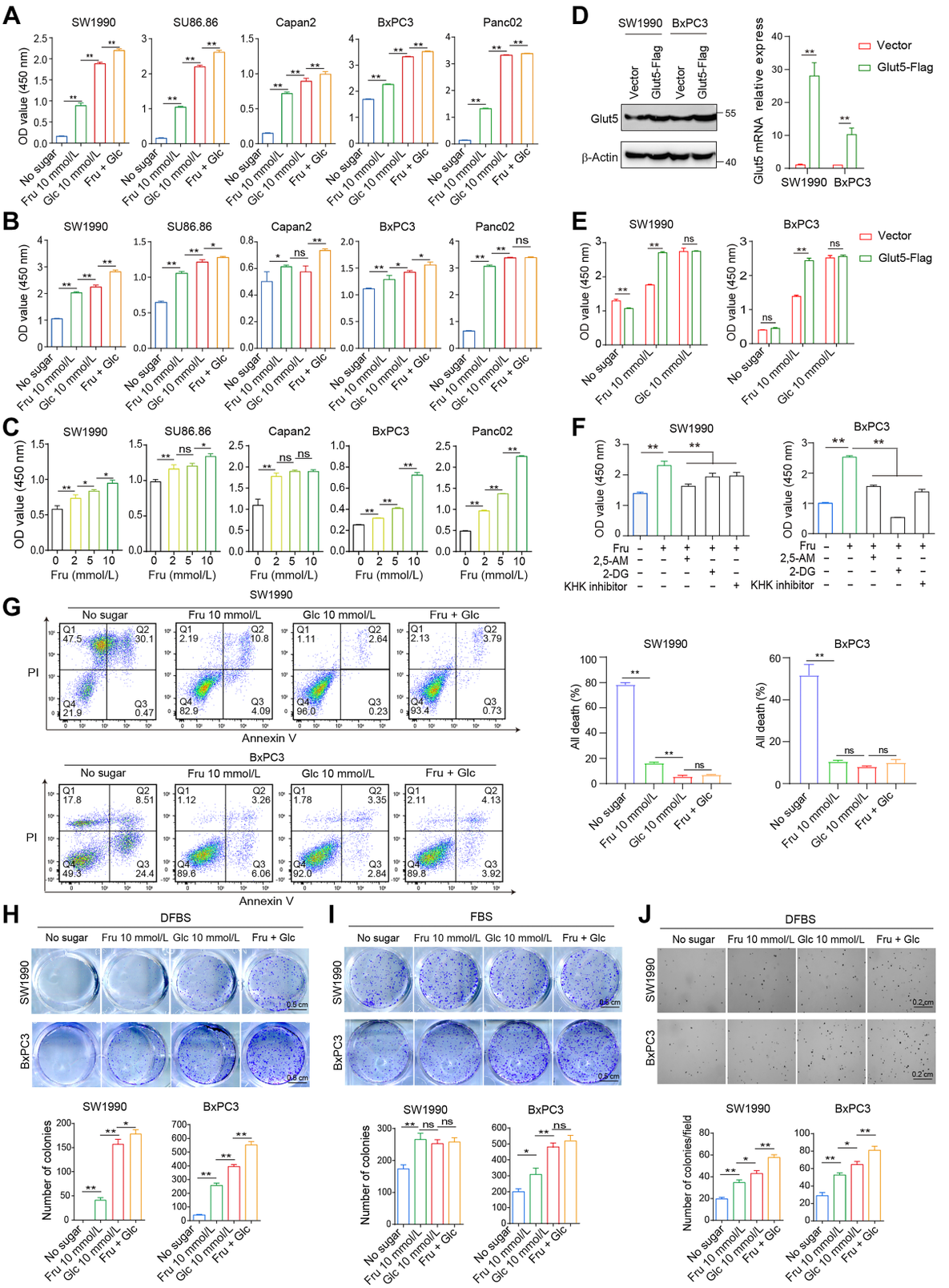
A
SW1990
SU86.86
Capan2
BxPC3
Panc02
OD value (450 nm)
No sugar
Fru 10 mmol/L
Glc 10 mmol/L
Fru + Glc
B
C
Fru (mmol/L)
D
Glut5
β-Actin
Vector
Glut5-Flag
Glut5 mRNA relative express
E
F
Fru
2,5-AM
2-DG
KHK inhibitor
G
PI
Annexin V
H
DFBS
I
FBS
J
Number of colonies
Number of colonies/field

cultured in different media at 37°C in 5% CO_2 for 16 hours. The width of the wound gap was photographed with an inverted microscope, and the relative migration distance was calculated using the Adobe Photoshop.

Transwell assay

Transwell assay was performed by using a Boyden chamber with a pore size of 8 μm as described previously (35). For cell migration assay, a total of 5×10^4 cells suspended in 200 μL of sugar-free medium were loaded onto the upper chambers and 500 μL of indicated media containing 10% FBS were added to the lower chamber. After incubation at 37°C for 24 hours, the migrated cells were fixed and stained. For cell invasion assay, a total of 5×10^4 cells suspended in 200 μL of glucose-free medium were loaded onto the upper chambers coated with Matrigel. After incubation at 37°C for 24 hours, the invaded cells were fixed, stained, and captured by a microscope.

Western blot analysis and antibodies

Western blot analysis was performed as described previously (36). Cell lysates were prepared with 1 × SDS lysis buffer, and then separated by SDS-PAGE and transferred to polyvinylidene difluoride (PVDF) membranes. After blocking in 5% skim milk for 1 hour, the PVDF membranes were incubated overnight at 4°C with corresponding primary antibodies. The following antibodies were used: AMPK [2532, Cell Signaling Technology (CST)], pAMPK (2535, CST), p70S6K (34475, CST), p-p70S6K (92434S, CST), Erk (4695S, CST), pErk (4370S, CST), AKt (9272, CST), pAkt (2965S, CST), SQSTM1/p62 (5114S, CST), LC3 (4108, CST), anti–O-GlcNAc antibody (PTM-952, PTM Biolabs), and β-actin (A1978, Sigma-Aldrich). The membranes were then incubated with the corresponding secondary antibodies for 1 hour at room temperature. Protein bands were detected using an ECL kit (Millipore) according to the manufacturer's instructions.

qRT-PCR analysis

RT-PCR was performed using a QRT-PCR kit (Vazyme, China) according to the manufacturer's instruction. In brief, total RNA was extracted by TRIzol, and then reverse transcribed into cDNA by HiScript II Q RT SuperMix for qPCR (Vazyme). The qPCR was performed using AceQ qPCR SYBR Green Master Mix (Vazyme) following the manufacturer's protocol. The gene expression was calculated by the $2^{-\Delta\Delta C_t}$ method. The following primers were used: Glut5, 5′-CAAGGATGCCA-ACAGTGATGAAGAG-3′ (forward) and 5′-GCAGAGTCGCCACAT-CATTTGA-3′ (reverse); β-actin: 5′-CAGAGCAAGAGAGGCATCC-3′ (forward) and 5′-CTGGGGTGTTGAAGGTCTC-3′ (reverse).

ATP production assay

ATP production was measured using an ATP assay kit (CellTiter-Glo Luminescent Cell Viability Assay cat: G7570) according to the manufacturer's protocol. Briefly, the cells were lysed with ATP assay lysis buffer and incubated for 10 minutes at room temperature, and then the supernatant was collected. Total ATP levels were calculated on the basis of the luminescence signal.

Metabolome analysis

Cells were cultured in Glc 5 mmol/L medium or Glc 5 mmol/L + Fru 10 mmol/L medium for 48 hours. Then the medium was removed and the cells were washed 3 times with pre-cooled PBS. Cellular metabolites were extracted in 1.5 mL of 80% prechilled methanol. After sonication for 6 minutes, the extracts were centrifuged at 5,000 rpm for 1 minute at 4°C, and then the supernatant was freeze-dried and dissolved in 10% methanol. Next, the solution was analyzed at Novogene Co., Ltd. using a Vanquish UHPLC system (Thermo Fisher Scientific) coupled with an Orbitrap Q Exactive TMHF-X mass spectrometer (Thermo Fisher Scientific). The metabolites were annotated using the Kyoto Encyclopedia of Genes and Genomes (KEGG), HMDB, and LIPIDMaps databases. Univariate analysis (t test) was applied to calculate the statistical significance. Metabolites with VIP > 1 and $P < 0.05$ and fold change (FC) ≥2 or ≤0.5 were considered significantly different. Volcano plots were used to filter metabolites of interest that based on $\log_2$ (fold change) and $-\log_{10}$ (P value) of metabolites by ggplot2 in R language. For clustering heat maps, the differential metabolite intensity areas were normalized using z-scores and ploted by the Pheatmap package in R language. The functions of these metabolites and metabolic pathways were studied using the KEGG database. The metabolic pathways enrichment of differential metabolites was performed, when ratio was satisfied by $x/n > y/N$, the metabolic pathway was considered as enrichment, when the P value of metabolic pathway was <0.05, the metabolic pathway was considered as statistically significant enrichment.

Mouse allograft models

Four- to five-week-old male C57BL/6 mice were purchased from Jiangsu Collective Pharmachem Biotechnology Co. A subcutaneous allograft model was established by subcutaneously injecting a total of 1×10^6 Panc02/luciferase cells in 100-μL saline solution. An orthotopic allograft model was established by intrapancreatic injection of a total of 5×10^5 Panc02/luciferase cells mixed in 50-μL saline solution and 50-μL Matrigel (BD Biosciences). For the PDAC liver metastasis model: Briefly, after general anesthesia, an approximately 1-cm incision was made in the left abdomen of the mice to expose the spleen, and then a total of 1×10^5 Panc02/luciferase cells suspension in 100 μL saline was injected into the spleen using a sterile syringe. After about 10 minutes, the spleen was resected and the skin incision was sutured. For the PDAC lung metastasis model, a total of 1×10^5 Panc02/luciferase cells suspension in 100 μL saline were injected into C57BL/6 mice through the tail vein. Each of the above mouse models was randomly divided

Figure 2.

Fructose contributes to the viability and colony-forming ability of PDAC cells *in vitro*. **A,** PDAC cell lines were cultured in the four indicated media containing 10% dialyzed FBS (DFBS) for 72 hours, and then cell viability was assessed by the CCK8 assay. **B,** CCK8 analysis was used to detect the viability of cells cultured in the above four media containing 10% FBS for 72 hours. **C,** The viability of PDAC cells cultured in glucose-free medium containing different concentrations of fructose for 72 hours was detected by CCK8. **D,** The expression levels of Glut5 in SW1990 and BxPC3 cell lines overexpressing Glut5 were verified by real-time PCR and Western blot. **E,** The viability of SW1990 and BxPC3 cells overexpressing Glut5 was assayed under different culture conditions. **F,** CCK8 analysis was used to detect the viability of SW1990 and BxPC3 cells cultured in fructose (10 mmol/L) medium in the presence of 2, 5-AM (3 mmol/L), 2-DG (2 mmol/L), or KHK inhibitor (1 μmol/L), respectively, for 48 hours. **G,** Apoptosis of SW1990 and BxPC3 was measured by flow cytometry under the four indicated conditions for 72 hours. **H** and **I,** Two-dimensional colony formation ability of SW1990 and BxPC3 cells was examined under the four indicated culture conditions containing DFBS (**H**) or FBS (**I**). **J,** Soft agar assay was performed to detect cell colony formation under the above four culture conditions in the presence of DFBS. All data are expressed as mean ± SD. Analysis was performed using one-way ANOVA followed by a Tukey test (**A**–**C** and **F**–**J**) or two-way ANOVA followed by a Tukey test (**D** and **E**); ns, nonsignificant; *, $P < 0.05$; **, $P < 0.01$.

into three groups and fed with distilled water, 10% glucose water or 10% fructose water, respectively. The water and diet intake was measured daily, and the weight of the mice was tested periodically. The IVIS Spectrum imaging system (PerkinElmer) was used to observe tumor growth and metastasis in each group. Depending on the imaging results and the progress of the experiment, mice were sacrificed to terminate the experiment. Afterwards, tumors, liver, and lungs of mice were collected, and fixed with 4% formaldehyde, embedded in paraffin. Then 4-μm sections were prepared for histological staining. All experimental operations followed the protocol approved by Tianjin Medical University Cancer Institute and Hospital, in accordance with the principles and procedures outlined in the NIH Guide for the Care and Use of Laboratory Animals.

H&E and IHC staining

Tissue slides were deparafffinized in xylene, dehydrated through gradient alcohol, and stained with hematoxylin and eosin (H&E) using routine staining procedures. For IHC staining, tissue slides were heated under high pressure in 0.01 mol/L sodium citrate (pH 6.0) for antigen retrieval, and endogenous peroxidase was blocked by 3% hydrogen peroxide solution. Then the slides were incubated with primary antibody at 4°C overnight and second antibody at room temperature for 1 hour. Subsequently, the sections were stained with diaminobenzidine (DAB) to visualize the immunolabeling. Antibodies against Glut5 (1:200, sc-271055, Santa Cruz), Ki67 (Beijing Zhongshan Jinqiao Biotechnology Co., Ltd.), cleaved caspase-3 (1:200, 9661S, CST), pAMPK (1:200, 2535, CST), and p-p70S6K (1:200, 92434S, CST) were used. The expression level of Glut5 was obtained by multiplying the percentage score of positive staining and the staining intensity score. The following percentage scores were defined: 1 (0%–25%), 2 (26%–50%), 3 (51%–75%), and 4 (76%–100%). The following intensity scores were defined: 0 (no staining), 1 (lower staining), 2 (moderate staining), and 3 (higher staining). All tissues were divided into high (score ≥ 6) and low (score < 6) groups according to the final score. For Ki67 and cleaved caspase-3, the expression level was determined by the percentage of positive cells.

Patients and tissue samples

A total of 129 cases of tissues were collected from patients diagnosed with PDAC at Tianjin Medical University Cancer Institute and Hospital between 2014 and 2016. Written informed consent was obtained from each patient. Retrospective clinicopathological information included sex, age, tumor size, lymph node status, TNM stage, pathological differentiation, and information on diabetes mellitus. Survival analysis was calculated using Kaplan–Meier analysis and Cox risk regression. Study was approved by the Ethics Committee of Tianjin Medical University Cancer Institute and Hospital, and conducted in accordance with the Declaration of Helsinki.

Public database

Glut5 mRNA expression levels in PDAC and normal pancreatic tissues were analyzed using Gene Expression Profiling Interactive Analysis (GEPIA, http://gepia.cancer-pku.cn/) of The Cancer Genome Atlas (TCGA) database. Glut5 protein expression levels in PDAC and normal pancreatic tissues were analyzed using the Human Protein Atlas (HPA) database (https://www.proteinatlas.org/). Survival analysis of PDAC in TCGA data was performed using GEPIA.

Statistical analysis

ANOVA between groups was performed in GraphPad Prism 8.3.0 software using unpaired *t* test, one-way or two-way ANOVA tests. The log-rank test was calculated in R language to determine the correlation between Glut5 expression and prognosis of patients with PDAC. The relationship between Glut5 expression and clinicopathological parameters was analyzed using the Statistical Package for Social Sciences (SPSS) 16.0 software (SPSS Inc.). $P < 0.05$ was considered statistically significant. All data are expressed as mean ± SD.

Data availability statement

The data that support the findings of this study are available from the corresponding author upon reasonable request. The public data of Glut5 mRNA and protein expression levels in PDAC and normal pancreatic tissues in this study were obtained from websites https://portal.gdc.cancer.gov, http://gepia2.cancer-pku.cn/#index and www.proteinatlas.org/.

Results

Glut5 is highly expressed in PDAC tissues and is associated with worse prognosis

Multiple studies have shown that Glut5 is expressed in tumor tissues and is associated with malignant tumor progression and patient prognosis (37). Our IHC results showed that Glut5 was dramatically upregulated in PDAC tissues (**Fig. 1A**). Consistently, analysis of the HPA and TCGA databases showed that Glut5 protein and transcript levels were extremely higher in PDAC tissues than in normal pancreatic tissues (**Fig. 1B** and **C**). Next, we divided 129 PDAC cases into Glut5 high- ($n = 74$) and low-expression groups ($n = 55$) based on the IHC score (**Fig. 1D**), and analyzed the relationship between Glut5 expression levels and the clinicopathological characteristics of the patients. Although there was no significant association between Glut5 expression level and pathological grade and clinical stage of pancreatic cancer and tumor metastasis (Supplementary Table S1), patients with PDAC with high Glut5 expression in tumor tissue had worse overall survival and 2- or 3-year survival rates (**Fig. 1E**). In addition, multivariate Cox regression analysis (model, including age, sex, clinical stage, pathological grade, tumor diameter, and Glut5 expression level) found that Glut5 expression level was an independent prognostic factor for patients with PDAC in addition to clinical stage (**Fig. 1F**). Meanwhile, analysis of TCGA database also showed that patients with high Glut5 mRNA expression had worse disease-free survival (**Fig. 1G** and **H**). Because diabetes is a known risk factor for PDAC and is inversely associated with the disease course (38), we also analyzed the relationship between Glut5 expression levels in PDAC tissues and patients with diabetes and found that patients with PDAC combined with diabetes had higher levels of Glut5 in their tumor tissues (**Fig. 1I**). Although no association was found between diabetes and the prognosis of patients with PDAC (**Fig. 1J**), patients with diabetes and high Glut5 expression had the worst prognosis (**Fig. 1K**). Taken together, these results powerfully suggest that Glut5 can be defined as an independent marker of disease progression in patients with PDAC.

Fructose contributes to the viability and colony-forming ability of PDAC cells *in vitro*

Next, we investigated the effect of fructose on the viability of a panel of PDAC cell lines *in vitro*, including KRAS mutant cell lines, such as SW1990, SU86.86, Capan2, Panc02, and KRAS wild-type cell line BxPC3. These cells were cultured in four kinds of media, including sugar-free medium (without fructose and glucose), glucose (Glc) medium (with 10 mmol/L glucose only), fructose (Fru) medium (with

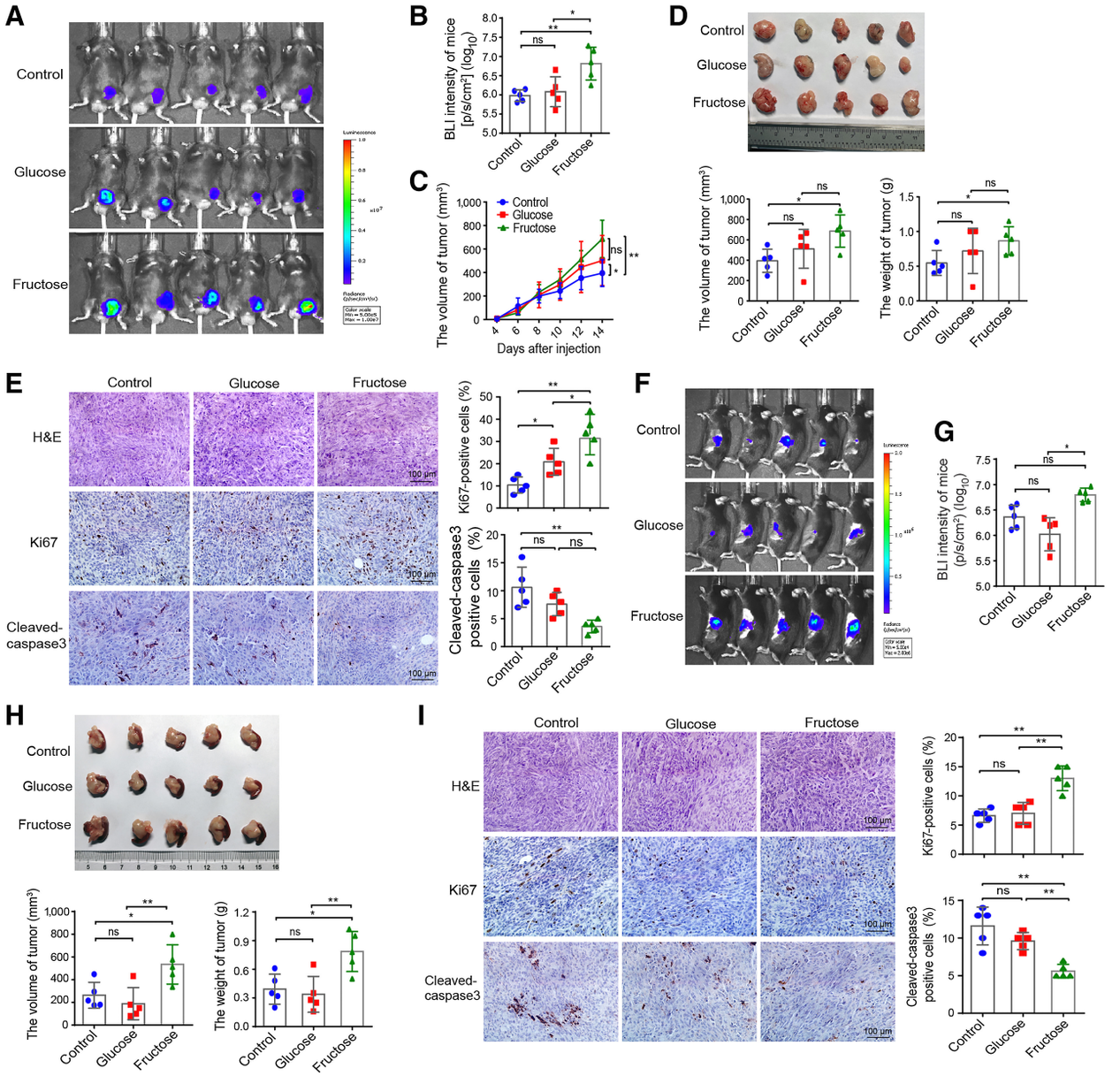

Figure 3.

Fructose promotes the growth of subcutaneous and orthotopic PDAC allograft tumors in mice. **A** and **B,** *In vivo* BLI images and values of subcutaneous tumor on day 14 after Panc02/luciferase cells injection in three groups (control, fructose, and glucose groups) of mice. **C,** The average tumor volume of tumor-bearing mice was measured over time after cell injection. **D,** Volume and weight of the excised tumor in the three groups of mice. **E,** Representative images of H&E and IHC staining (×400), and statistical results of Ki67 and cleaved caspase-3 expressions in tumor tissues. **F** and **G,** *In vivo* BLI images and values of orthotopic graft tumors in the pancreas on day 10 after injection of Panc02/luciferase cells in three groups of mice. **H,** Volume and weight of the excised tumors in orthotopic allograft mouse model. **I,** Representative images of H&E and IHC staining (×400), and statistical results of Ki67 and cleaved caspase-3 expressions in the orthotopic graft tumor tissues. All data are shown as mean ± SD. Analysis was performed using one-way ANOVA followed by a Tukey test; ns, nonsignificant; *, $P < 0.05$; **, $P < 0.01$; $n = 5$ for the *in vivo* experiments.

10 mmol/L fructose only), and double-sugar medium (with 10 mmol/L fructose and 10 mmol/L glucose), and cell viability assays showed that fructose enabled cells to survive in medium containing 10% dialyzed FBS (DFBS, **Fig. 2A**) and medium containing 10% FBS (**Fig. 2B**). Although fructose was not as effective as glucose in supporting cell survival in some cell lines, double-sugar medium promoted cell viability more efficiently (Supplementary Fig. S1B; **Fig. 2A** and **B**). Moreover, the addition of different concentrations of fructose to the glucose medium increased cell viability, and fructose promoted cell viability in a linear dose–response manner (Supplementary Fig. S1C; **Fig. 2C**). To investigate whether Glut5 confers fructose-driven cell proliferation, we constructed two cell lines with high Glut5

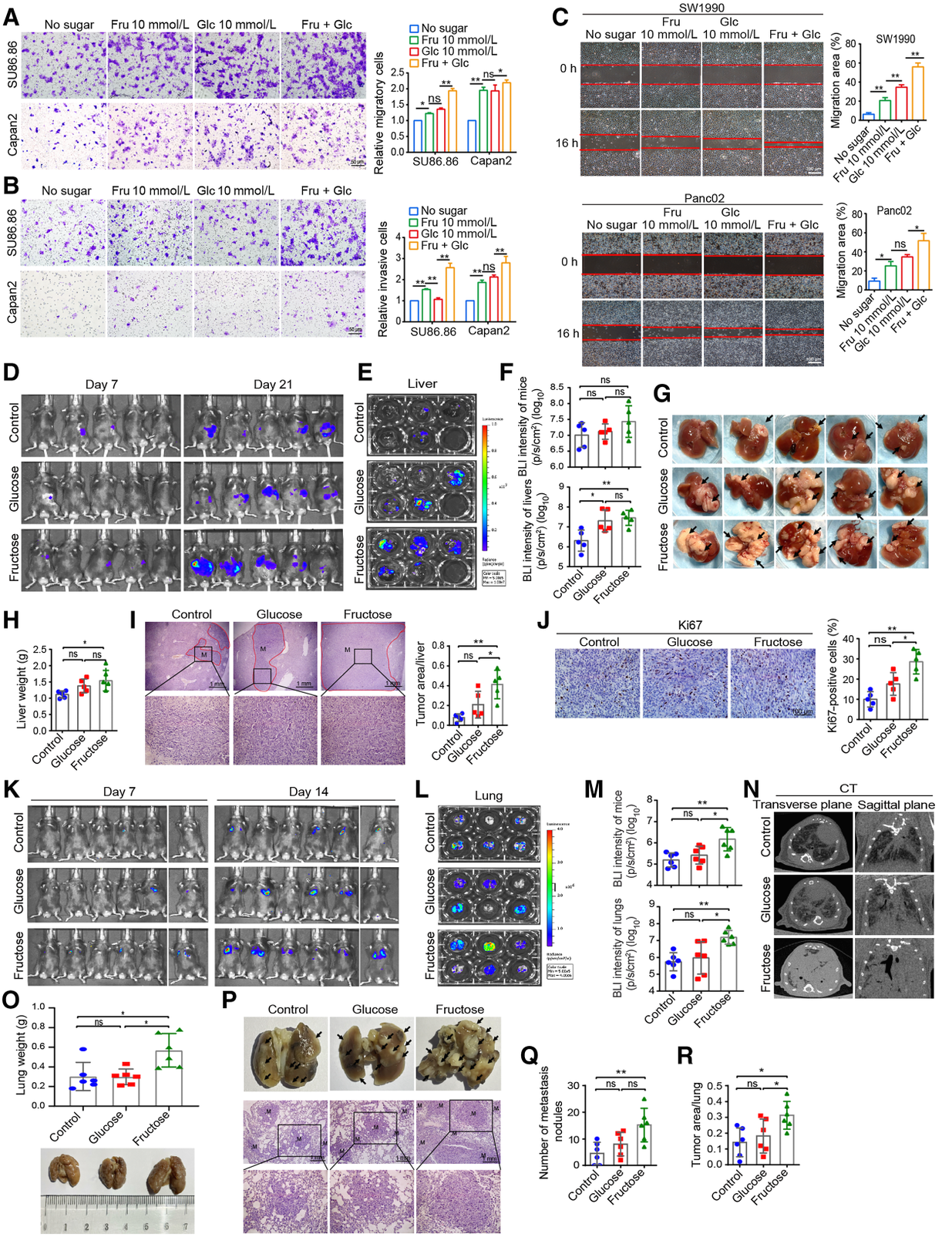
A
No sugar
Fru 10 mmol/L
Glc 10 mmol/L
Fru + Glc
SU86.86
Capan2
Relative migratory cells
SU86.86
Capan2
B
Relative invasive cells
C
SW1990
Fru
Glc
0 h
16 h
Migration area (%)
Panc02
D
Day 7
Day 21
Control
Glucose
Fructose
E
Liver
F
BLI intensity of mice (p/s/cm²) (log10)
BLI intensity of livers (p/s/cm²) (log10)
G
H
Liver weight (g)
I
Tumor area/liver
J
Ki67
Ki67-positive cells (%)
K
Day 14
L
Lung
M
BLI intensity of lungs (p/s/cm²) (log10)
N
CT
Transverse plane
Sagittal plane
O
Lung weight (g)
P
Q
Number of metastasis nodules
R
Tumor area/lung

expression (**Fig. 2D**). High expression of Glut5 in SW1990 and BxPC3 cells enhanced the ability of fructose to promote cell viability (**Fig. 2E**). On the contrary, inhibition of Glut5 by 2, 5-AM (2, 5-anhydro-D-mannitol) or silencing of Glut5 by shRNA reduced cell viability in fructose medium, but not in glucose medium (**Fig. 2F**; Supplementary Fig. S1D–S1F). Similar results were obtained when fructolysis inhibitors 2-DG (HK inhibitor) or KHK inhibitor was present in the culture medium (**Fig. 2F**; Supplementary Fig. S1D). Moreover, fructose also effectively suppressed sugar deprivation-induced cell death (**Fig. 2G**). Hypoxia is a prominent feature of PDAC, therefore, we further determined the effect of fructose on cell viability under hypoxia. Fructose effectively promoted cell viability (Supplementary Fig. S2A) and inhibited cell death (Supplementary Fig. S2B), and this effect was more prominent in PDAC cells overexpressing Glut5 (Supplementary Fig. S2C and S2D).

Then, clonogenetic assay was performed to evaluate the proliferative capacity of individual cells. PDAC cells were barely able to form colonies in sugar-free medium with DFBS, but cells cultured in fructose medium exhibited greater clonogenicity (**Fig. 2H**). In addition, PDAC cells can form small colonies in sugar-free medium with FBS, whereas these cells produced more and larger colonies in the presence of fructose (**Fig. 2I**). Although glucose was more conducive to cell colony formation than fructose, PDAC cells showed the strongest colony formation in the double-sugar medium containing DFBS (**Fig. 2H** and **I**). In addition, the colony-forming ability of PDAC cells in fructose medium was extremely suppressed in the presence of 2, 5-AM or fructolysis inhibitors (Supplementary Fig. S3A and S3B), whereas it was enhanced in Glut5-overexpressing cells (Supplementary Fig. S3C). Moreover, fructose also stimulated anchorage-independent growth ability of PDAC cells on soft agar (**Fig. 2J**). Collectively, fructose can maintain the proliferation of PDAC cells in the absence of glucose.

Increased fructose intake accelerates the growth of PDAC allografts in mice

To examine the effect of fructose intake on tumor growth *in vivo*, we established subcutaneous allograft and pancreatic orthotopic graft tumor models by injecting Panc02/luciferase cells into C57BL/6 mice. After tumor cell inoculation, all mice were randomly divided into three groups and administered with different drinking water—the control (fed with normal water), fructose (fed with 10% fructose water), and glucose groups (fed with 10% glucose water). Water and food intake was measured daily, and there were no significant differences among the three groups (Supplementary Fig. S4A). In the subcutaneous allograft model, *in vivo* bioluminescence imaging (BLI; **Fig. 3A** and **B**) combined with *in vitro* tumor volume measurement (**Fig. 3C**) was used to detect tumor growth, and the results showed that fructose feeding significantly promoted the growth of subcutaneous tumors in mice compared with the control group, but did not differ from the glucose-fed group. For harvested tumors, both volume and weight of the fructose-fed group were greater than those of the control group (**Fig. 3D**). Although the difference in tumor volume between the fructose and the glucose groups was not statistically significant, the BLI values of the fructose group were extremely higher than those of the glucose group (**Fig. 3A** and **B**). Moreover, IHC staining analysis of Ki67 and cleaved caspase-3 showed that the proliferative activity of Panc02 cells was significantly increased and the apoptosis rate was substantially decreased in tumor sections from fructose-fed mice (**Fig. 3E**). On the contrary, silencing of Glut5 significantly reduced tumor growth in the fructose-fed mice (Supplementary Fig. S4B–S4D). In mouse orthotopic allograft models, fructose was found to promote tumor growth by detecting BLI *in vivo* (**Fig. 3F** and **G**) and measuring the volume and weight of harvested tumors (**Fig. 3H**). Interestingly, fructose was more likely to facilitate tumor growth than glucose in this model (**Fig. 3F–H**). In addition, the tumor proliferation index was the highest and the apoptosis rate was the lowest in the fructose group (**Fig. 3I**). Collectively, these data demonstrate that fructose is crucial for PDAC development and progression *in vivo*.

Fructose promotes invasion and metastasis of PDAC cells *in vitro* and *in vivo*

Early metastasis is one of the characteristics of PDAC (5). In this study, the migration and invasion abilities of SU86.86 and Capan2 cells were significantly higher in fructose medium than in glucose-free medium, whereas the cells in double-sugar medium had the strongest migration and invasion abilities (**Fig. 4A** and **B**). Meanwhile, similar results were obtained in wound-healing assay with SW1990 and Panc02 cells, suggesting that fructose significantly promoted the migration of PDAC cells (**Fig. 4C**). Moreover, the migration ability of SW1990 cells in fructose medium was extremely suppressed in the presence of inhibiting Glut5 or fructolysis inhibitors (Supplementary Fig. S4E and S4F), and was upregulated by overexpression of Glut5 in PDAC cells (Supplementary Fig. S4G).

We next constructed mouse models of liver metastasis by spleen injection of Panc02/luciferase cells and mouse models of lung metastasis by tail vein injection of Panc02/luciferase cells. As in the previous models, we randomly divided the mice into three groups according to the feeding method. In the liver metastasis model, although the BLI intensity of these three groups of mice was not significantly different, the BLI intensity and weight of isolated livers were significantly higher in the fructose and glucose groups than in the control

Figure 4.

Fructose promotes invasion and metastasis of PDAC cells. **A** and **B,** The migratory (**A**) and invasive (**B**) abilities of SU86.86 and Capan2 cells were determined by Transwell assay in the four media used in the above experiments. **C,** Wound-healing analysis of the migration ability of SW1990 and Panc02 cells under the four indicated conditions. **D,** Bioluminescence imaging of three groups of mice on day 21 in the tumor metastasis model with splenic injection of Panc02/luciferase cells. **E,** Imaging of the excised livers of the above three groups of mice. **F,** Statistical analysis of BLI intensity of mice (**D**) and the excised livers (**E**). **G,** Representative images of the excised livers of each group. Black arrows, tumor metastasis nodules on the liver surface. **H,** The weight of the excised livers in each group of mice. **I,** Representative images of H&E staining of the liver (×40 and ×200) and the proportion of tumor area in the whole liver of the three groups. **J,** Representative images of Ki67 staining in liver metastases (×400) and corresponding statistical results. **K,** *In vivo* imaging of mice in three groups on days 7 and 14 after tail vein injection of Panc02/luciferase cells. The imaging system can only detect a maximum of 5 mice at a time, so the sixth mouse in each group was detected alone. **L,** Imaging of isolated lungs of the above three groups. **M,** BLI intensity of mice in **Fig. 3K** and lungs in **Fig. 3L**. **N,** Representative micro-CT images of the lungs from each group. **O,** Weight of isolated lungs from each group. **P,** Representative images of isolated lungs from each group (black arrows, tumor metastatic nodules on the lung surface) and H&E-staining images of lung tissue sections (×40 and ×200). M, the tumor metastasis. **Q,** The metastatic nodules in the lungs of different groups. **R,** Proportion of tumor area in the total lungs of three groups. All data are shown as mean ± SD. Analysis was performed using one-way ANOVA followed by a Tukey test; ns, nonsignificant; *, $P < 0.05$; **, $P < 0.01$; $n = 3$ in cell experiments, $n = 5$ in liver metastasis model, and $n = 6$ in lung metastasis model.

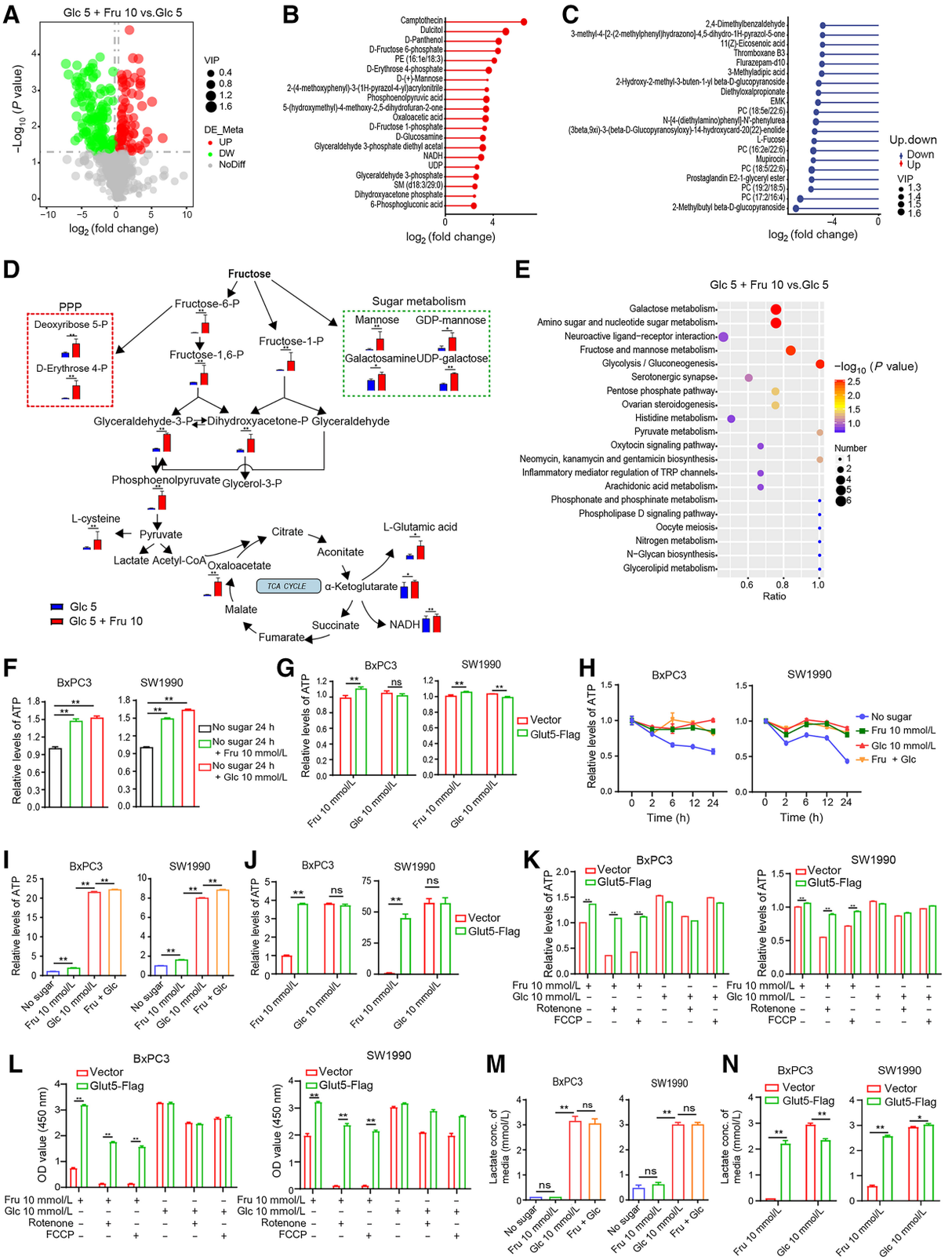
A
Glc 5 + Fru 10 vs.Glc 5
−Log10 (P value)
log2 (fold change)
VIP
0.4
0.8
1.2
1.6
DE_Meta
UP
DW
NoDiff
B
Camptothecin
Dulcitol
D-Panthenol
D-Fructose 6-phosphate
PE (16:1e/18:3)
D-Erythrose 4-phosphate
D-(+)-Mannose
2-(4-methoxyphenyl)-3-(1H-pyrazol-4-yl)acrylonitrile
Phosphoenolpyruvic acid
5-(hydroxymethyl)-4-methoxy-2,5-dihydrofuran-2-one
Oxaloacetic acid
D-Fructose 1-phosphate
D-Glucosamine
Glyceraldehyde 3-phosphate diethyl acetal
NADH
UDP
Glyceraldehyde 3-phosphate
SM (d18:3/29:0)
Dihydroxyacetone phosphate
6-Phosphogluconic acid
log2 (fold change)
C
2,4-Dimethylbenzaldehyde
3-methyl-4-[2-(2-methylphenyl)hydrazono]-4,5-dihydro-1H-pyrazol-5-one
11(Z)-Eicosenoic acid
Thromboxane B3
Flurazepam-d10
3-Methyladipic acid
2-Hydroxy-2-methyl-3-buten-1-yl beta-D-glucopyranoside
Diethyloxalpropionate
EMK
PC (18:5e/22:6)
N-[4-(diethylamino)phenyl]-N'-phenylurea
(3beta,9xi)-3-(beta-D-Glucopyranosyloxy)-14-hydroxycard-20(22)-enolide
L-Fucose
PC (16:2e/22:6)
Mupirocin
PC (18:5/22:6)
Prostaglandin E2-1-glyceryl ester
PC (19:2/18:5)
PC (17:2/16:4)
2-Methylbutyl beta-D-glucopyranoside
Up.down
Down
Up
VIP
1.3
1.4
1.5
1.6
log2 (fold change)
D
Fructose
PPP
Deoxyribose 5-P
D-Erythrose 4-P
Fructose-6-P
Fructose-1,6-P
Fructose-1-P
Sugar metabolism
Mannose
GDP-mannose
GalactosamineUDP-galactose
Glyceraldehyde-3-P
Dihydroxyacetone-P
Glyceraldehyde
Phosphoenolpyruvate
Glycerol-3-P
L-cysteine
Pyruvate
Lactate
Acetyl-CoA
Citrate
Aconitate
L-Glutamic acid
Oxaloacetate
TCA CYCLE
α-Ketoglutarate
Malate
Succinate
NADH
Fumarate
Glc 5
Glc 5 + Fru 10
E
Glc 5 + Fru 10 vs.Glc 5
Galactose metabolism
Amino sugar and nucleotide sugar metabolism
Neuroactive ligand−receptor interaction
Fructose and mannose metabolism
Glycolysis / Gluconeogenesis
Serotonergic synapse
Pentose phosphate pathway
Ovarian steroidogenesis
Histidine metabolism
Pyruvate metabolism
Oxytocin signaling pathway
Neomycin, kanamycin and gentamicin biosynthesis
Inflammatory mediator regulation of TRP channels
Arachidonic acid metabolism
Phosphonate and phosphinate metabolism
Phospholipase D signaling pathway
Oocyte meiosis
Nitrogen metabolism
N−Glycan biosynthesis
Glycerolipid metabolism
−log10 (P value)
Number
Ratio
F
BxPC3
SW1990
Relative levels of ATP
No sugar 24 h
No sugar 24 h + Fru 10 mmol/L
No sugar 24 h + Glc 10 mmol/L
G
BxPC3
SW1990
Relative levels of ATP
Vector
Glut5-Flag
Fru 10 mmol/L
Glc 10 mmol/L
H
BxPC3
SW1990
Relative levels of ATP
Time (h)
No sugar
Fru 10 mmol/L
Glc 10 mmol/L
Fru + Glc
I
BxPC3
SW1990
Relative levels of ATP
No sugar
Fru 10 mmol/L
Glc 10 mmol/L
Fru + Glc
J
BxPC3
SW1990
Relative levels of ATP
Vector
Glut5-Flag
Fru 10 mmol/L
Glc 10 mmol/L
K
BxPC3
SW1990
Vector
Glut5-Flag
Relative levels of ATP
Fru 10 mmol/L
Glc 10 mmol/L
Rotenone
FCCP
L
BxPC3
SW1990
Vector
Glut5-Flag
OD value (450 nm)
Fru 10 mmol/L
Glc 10 mmol/L
Rotenone
FCCP
M
BxPC3
SW1990
Lactate conc. of media (mmol/L)
No sugar
Fru 10 mmol/L
Glc 10 mmol/L
Fru + Glc
N
BxPC3
SW1990
Vector
Glut5-Flag
Lactate conc. of media (mmol/L)
Fru 10 mmol/L
Glc 10 mmol/L

group (**Fig. 4D–F**). Moreover, more liver surface metastases (**Fig. 4G**) and heavier liver (**Fig. 4H**) appeared in the fructose and glucose groups, and H&E staining also confirmed that fructose and glucose promoted liver metastasis of Panc02 cells, with more metastatic foci found in the fructose group than in the glucose group (**Fig. 4I**). In addition, the cell proliferation index was also higher in the metastases in the fructose group (**Fig. 4J**). Although silencing of Glut5 obviously inhibited tumor metastasis in the fructose-fed mice (Supplementary Fig. S4H–S4J). In the lung metastasis model, the BLI intensity was particularly stronger in mice and isolated lungs in the fructose group than in the other two groups (**Fig. 4K–M**), suggesting that fructose significantly promoted the metastasis of PDAC cells. Consistently, CT imaging also confirmed the above results (**Fig. 4N**). Meanwhile, the lungs of the mice in the fructose group were the largest and heaviest (**Fig. 4O**), and H&E staining also revealed that the fructose group had more metastatic nodules and tumor area in the lungs than the other two groups (**Fig. 4P–R**).

Fructose provides available carbon sources and ATP for PDAC cells

To further elucidate how PDAC cells use fructose, we compared the metabolic changes in cells cultured in media containing 5 mmol/L Glc or 5 mmol/L Glc + 10 mmol/L Fru, which simulate sugar concentrations under physiological conditions *in vivo*. The volcano (**Fig. 5A**) and heat maps (Supplementary Fig. S5A) clearly showed the relative amounts of the differential metabolites. Among these metabolites, D-fructose 6-phosphate, D-fructose 1-phosphate, phosphoenolpyruvic acid, glyceraldehyde-3-phosphate, dihydroxyacetone phosphate, oxaloacetic acid, D-erythrose 4-phosphate, D-mannose, and NADH were significantly upregulated in the Glc 5 + Fru 10 group and distributed among the top 20 most significantly upregulated metabolites (**Fig. 5B**), whereas a variety of unsaturated fatty acids were found among the top 20 downregulated metabolites (**Fig. 5C**). Combining the metabolic pathways of fructose (**Fig. 5D**) and the metabolomics results, we found a significant upregulation of the levels of ribose, amino acids, and other sugars (e.g., mannose and galactose) in addition to metabolites of glycolysis and the tricarboxylic acid cycle (TCA cycle). Consistently, pathway enrichment analysis showed that fructose and mannose metabolism, glycolysis, gluconeogenesis, pentose phosphate (PPP) pathway, galactose pathway, and amino sugar and nucleotide sugar metabolism were all significantly changed (**Fig. 5E**). These results suggest that fructose increases the intermediate metabolites of intracellular glycolysis, TCA, and PPP pathways, and upregulates the levels of amino sugars, nucleotide sugars, and other sugars. Furthermore, the metabolism of galactose, amino sugars, and nucleotide sugars was the most abundant pathways in the Glc 5 + Fru 10 group (**Fig. 5E**), indicating that these metabolic changes may affect the glycosylation of intracellular proteins, and indeed, cells in the Glc 5 + Fru 10 group showed increased levels of glycosylation, especially for macromolecular proteins and histones (Supplementary Fig. S5B and S5C).

ATP is known to be essential for all aspects of cellular activity. Our results showed that both glucose and fructose significantly restored the reduction of intracellular ATP caused by glucose deficiency in BxPC3 and SW1990 cells (**Fig. 5F**), and fructose upregulated ATP levels in a concentration-dependent pattern (Supplementary Fig. S5D). Moreover, compared with control cells, overexpression of Glut5 in PDAC cells increased ATP production in fructose medium (**Fig. 5G**). At the same time, we compared the ATP levels of PDAC cells in the four indicated media at different time points and found that the ATP levels in the three media were constant except for the sugar-free medium, and there was no significant difference between the three media (**Fig. 5H**). Intracellular ATP levels were also higher in fructose medium than in sugar-free medium but lower than in glucose medium under hypoxia (**Fig. 5I**), which was different from the results under normoxia. Moreover, the OXPHOS inhibitors, FCCP, and rotenone, downregulated intracellular ATP levels more obviously in fructose medium than in glucose medium under normoxia (Supplementary Fig. S5E). Nevertheless, a different phenomenon occurred in cells overexpressing Glut5, which effectively maintained higher ATP levels in fructose medium under hypoxia (**Fig. 5J**) or in the presence of OXPHOS inhibitors (**Fig. 5K**), and this phenomenon was also seen in cells from other cancer types (Supplementary Fig. S5F). Meanwhile, the inhibitory effects of FCCP and rotenone on ATP production were attenuated in PDAC cell lines (SU86.86 and Capan2) with high endogenous Glut5 level compared with cell lines with low Glut5 expression (SW1990, BxPC3, and Panc02; Supplementary Fig. S5E and S5G). Hence, these results suggest that OXPHOS is the major ATP supplier in PDAC cells cultured in fructose medium, whereas fructolysis is the major ATP supplier in PDAC cells overexpressing Glut5. Probably for this reason, the viability of the control cells in fructose medium containing rotenone or FCCP was significantly decreased compared with the Glut5-overexpressing cells (**Fig. 5L**; Supplementary Fig. S5H). Likewise, PDAC cells produced barely detectable lactate in fructose medium, but overexpression of Glut5 in these cells significantly increased lactate production, approaching lactate levels in glucose medium (**Fig. 5M** and **N**). All these results indicate that high Glut5 expression causes a metabolic reprogramming and induces fructose metabolism in favor of the glycolytic pathway. As a possible cause, analysis of the TCGA database showed that Glut5 transcript expression was positively correlated with the glycolysis-associated gene set

Figure 5.

Fructose provides sufficient carbon sources for PDAC cells and maintains high levels of intracellular ATP. **A,** Volcano plots showing all identified metabolites in two groups obtained by metabolomics analysis. Each dot represents a metabolite with a different color indicating downregulated (green), upregulated (red), or non-significant (gray) metabolites (FDR adjusted *P* value < 0.05) with >2-fold change. **B,** The top 20 most significantly upregulated metabolites in the Glc 5 + Fru 10 group. **C,** The top 20 significantly downregulated metabolites in the Glc 5 + Fru 10 group. **D,** Pathway map of some significantly different metabolites between Glc 5 and Glc 5 + Fru 10 groups. The blue and red histograms indicate the content of metabolites in the Glc 5 and Glc 5 + Fru 10 groups, respectively. **E,** Overview of enrichment analysis based on metabolite alterations. **F,** Effect of fructose and glucose on intracellular ATP levels in SW1990 and BxPC3 cells after sugar starvation for 24 hours. **G,** Relative ATP levels of SW1990 and BxPC3 cells were examined at different time points under the four indicated culture conditions containing DFBS. **H,** ATP levels in Glut5-overexpressing and control cells under different culture conditions. **I,** Relative ATP levels in SW1990 and BxPC3 cells cultured in the four conditions under hypoxia for 12 hours. **J,** Relative ATP levels of Glut5-overexpressing and control cells cultured under hypoxic conditions for 2 hours under different conditions. **K,** Relative ATP levels of Glut5-overexpressing and control cells cultured for 2 hours under different conditions in the presence of rotenone (10 μmol/L) or FCCP (10 μmol/L). **L,** Viability of Glut5-overexpressing and control cells cultured for 24 hours under different conditions in the presence of rotenone (10 μmol/L) or FCCP (10 μmol/L). **M,** Lactate concentrations in the media of SW1990 and BxPC3 cells cultured for 12 hours under different culture conditions. **N,** Lactate concentrations in media from Glut5-overexpressing and control cells cultured for 12 hours under different conditions. All data are shown as mean ± SD. Analysis was performed using an unpaired Student *t* test (**D**) or one-way ANOVA followed by a Tukey test (**F**, **I**, and **M**) or two-way ANOVA followed by a Tukey test (**G**, **J**, **K**, **L**, and **N**); ns, non-significant; *, $P < 0.05$; **, $P < 0.01$; $n = 3$.

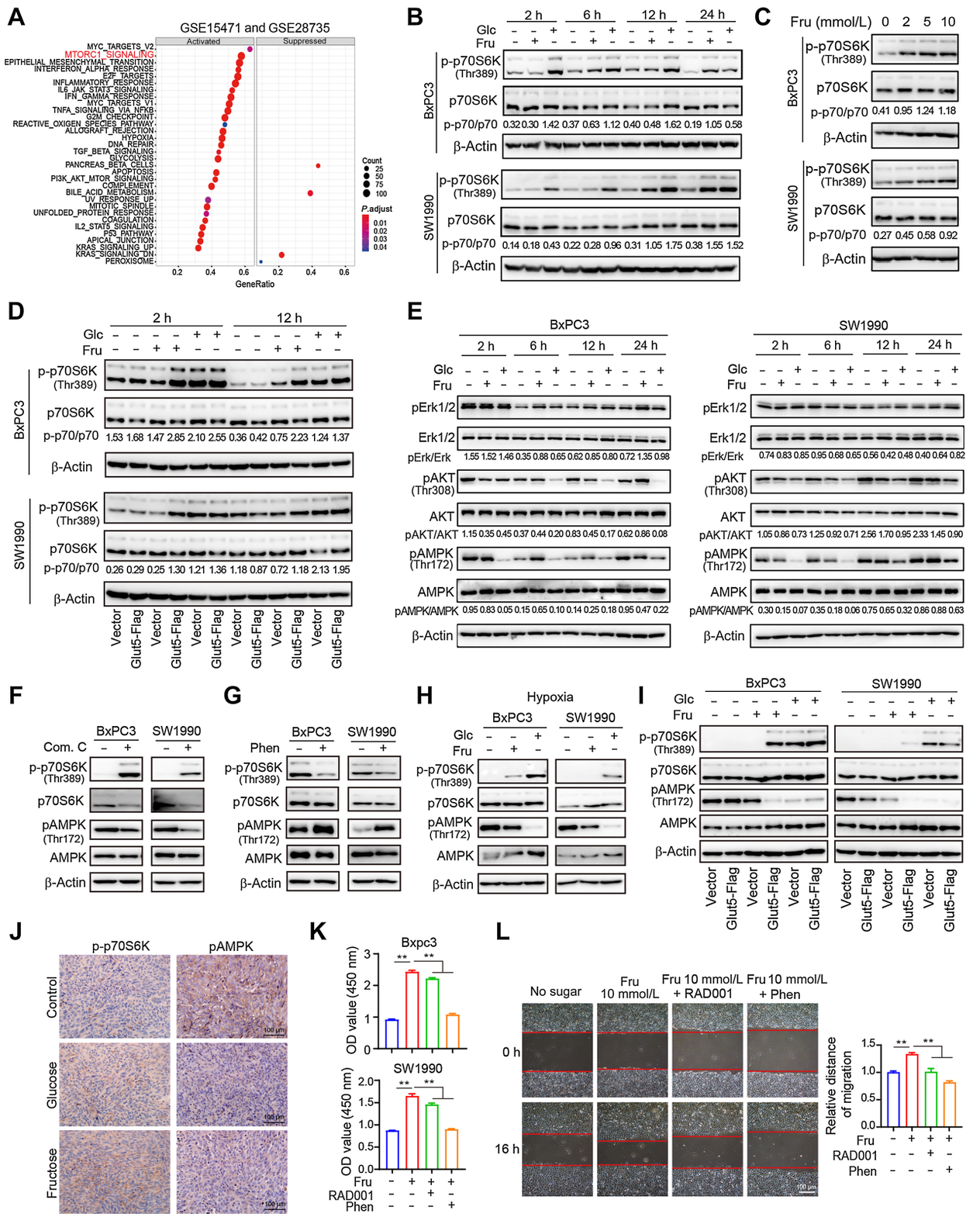
A
GSE15471 and GSE28735
Activated
Suppressed
MYC_TARGETS_V2
MTORC1_SIGNALING
EPITHELIAL_MESENCHYMAL_TRANSITION
INTERFERON_ALPHA_RESPONSE
E2F_TARGETS
INFLAMMATORY_RESPONSE
IL6_JAK_STAT3_SIGNALING
IFN_GAMMA_RESPONSE
MYC_TARGETS_V1
TNFA_SIGNALING_VIA_NFKB
G2M_CHECKPOINT
REACTIVE_OXIGEN_SPECIES_PATHWAY
ALLOGRAFT_REJECTION
HYPOXIA
DNA_REPAIR
TGF_BETA_SIGNALING
GLYCOLYSIS
PANCREAS_BETA_CELLS
APOPTOSIS
PI3K_AKT_MTOR_SIGNALING
COMPLEMENT
BILE_ACID_METABOLISM
UV_RESPONSE_UP
MITOTIC_SPINDLE
UNFOLDED_PROTEIN_RESPONSE
COAGULATION
IL2_STAT5_SIGNALING
P53_PATHWAY
APICAL_JUNCTION
KRAS_SIGNALING_UP
KRAS_SIGNALING_DN
PEROXISOME
GeneRatio
Count
P.adjust
B
2 h
6 h
12 h
24 h
Glc
Fru
BxPC3
SW1990
p-p70S6K (Thr389)
p70S6K
p-p70/p70
β-Actin
C
Fru (mmol/L) 0 2 5 10
D
Vector
Glut5-Flag
E
pErk1/2
Erk1/2
pErk/Erk
pAKT (Thr308)
AKT
pAKT/AKT
pAMPK (Thr172)
AMPK
pAMPK/AMPK
F
Com. C
G
Phen
H
Hypoxia
I
J
p-p70S6K
pAMPK
Control
Glucose
Fructose
K
Bxpc3
OD value (450 nm)
L
No sugar
Fru 10 mmol/L
Fru 10 mmol/L + RAD001
Fru 10 mmol/L + Phen
0 h
16 h
Relative distance of migration
RAD001
Phen

(Supplementary Fig. S5I) and negatively correlated with that of OXPHOS (Supplementary Fig. S5J), which may explain the above phenomenon.

Fructose maintains activation of the mTORC1 signaling pathway in PDAC cells

To elucidate the mechanisms by which fructose utilization regulates the biological function of PDAC cells, Gene Set Enrichment Analysis was conducted in two independent pancreatic cancer datasets, GEO (GSE15471 and GSE28735) and TCGA. The results showed that the mTORC1 pathway was enriched in PDAC with high Glut5 mRNA expression (**Fig. 6A**; Supplementary Fig. S6A). To verify this possibility, we compared the activation of p70S6 kinase (p70S6K), a downstream kinase of the mTORC1 pathway, in BxPC3 and SW1990 cells at the same time points (2, 6, 12, and 24 hours) in fructose, glucose, and sugar-free medium. We found that p70S6K was significantly activated in cells cultured with fructose or glucose (**Fig. 6B**). In addition, fructose activated p70S6K in a concentration-dependent manner (**Fig. 6C**), and p70S6K activation was more pronounced in cells overexpressing Glut5 (**Fig. 6D**) and weaker in cells in which Glut5 was inhibited (Supplementary Fig. S6B and S6C). Meanwhile, the activation of AKT and ERK (the main upstream signals of mTORC1) was not altered, whereas the activation of AMPK was significantly inhibited (**Fig. 6E**). Furthermore, the AMPK inhibitor Compound C (Com. C) upregulated p70S6K activation in PDAC cells cultured in sugar-free medium (**Fig. 6F**), whereas the AMPK activator phenformin (Phen) extremely inhibited p70S6K activation in cells cultured in fructose medium (**Fig. 6G**), suggesting that fructose-induced activation of p70S6K is dependent on its inhibitory effect on AMPK activity. Similarly, fructose inhibited the activation of AMPK in PDAC cells under hypoxia, but activated p70S6K (**Fig. 6H**), and this effect was significantly enhanced in cells overexpressing Glut5 (**Fig. 6I**). In addition, the activation of AMPK was inhibited and p70S6K was activated in allogeneic subcutaneous tumor tissues in the glucose and fructose groups compared with the control group (**Fig. 6J**). Moreover, the proliferation and migration abilities of PDAC cells cultured in fructose medium were significantly inhibited in the presence of the mTORC1 inhibitor RAD001 or the AMPK activator Phen (**Fig. 6K** and **L**). Collectively, fructose affects the biological function of PDAC cells mainly by regulating the AMPK–mTORC1 signaling pathway.

Fructose reduces sugar-free–induced cell death by inhibiting autophagy

Sugar deprivation has been reported to induce autophagy and autophagic cell death (39). Consistently, the addition of the autophagy inhibitor chloroquine to the sugar-free medium inhibited cell death (**Fig. 7A**). To determine whether fructose reversal of sugar starvation–induced cell death is associated with inhibition of autophagy, we constructed a BxPC3 cell line expressing GFP-LC3 and subjected the cells to 24 hours of sugar starvation followed by fructose supplementation. As shown in **Fig. 7B**, fructose significantly inhibited sugar deprivation–induced autophagy as measured by GFP–LC3 fluorescent spots and LC3II/I levels. Subsequently, we compared the effects of fructose and glucose on autophagy under the same conditions and further demonstrated that fructose could inhibit sugar-free–induced autophagy with similar effects as glucose (**Fig. 7C**). Consistently, measurements of the LC3II/I ratio and P62 levels also confirmed that fructose inhibited autophagy similarly to glucose (**Fig. 7D**). However, under glucose-sufficient conditions, fructose did not affect the LC3II/I ratio and p62 protein expression, suggesting that fructose only affects autophagy induced by glucose deficiency (**Fig. 7E**). Considering that fructose increases various intracellular metabolites, upregulates ATP levels, and maintains the activity of the mTORC1 signaling, these changes are intimately related to autophagy. Therefore, we speculated that fructose may affect the autophagic process through the mTORC1 signaling. As expected, the mTORC1 inhibitor RAD001 and the AMPK activator Phen significantly prevented the inhibitory effect of fructose on autophagy in fructose medium (**Fig. 7F**). Moreover, the presence of 2, 5-AM or fructolysis inhibitors in fructose medium remarkably increased autophagy induced by sugar starvation (**Fig. 7G**). Collectively, fructose efficiently inhibits excessive autophagy caused by sugar deprivation.

Discussion

Elevated metabolic activity and/or restricted blood supply in tumor tissue can lead to severe deficiencies of multiple nutrients, especially glucose, and therefore tumor cells must reprogram their metabolism to use all available carbon sources whenever possible (40, 41). The remarkable tumor desmoplasia and minimal vascularity in PDAC tissue exacerbate nutritional deficiency of the tumor, making increased utilization of anaplerotic carbon sources and activation of bypass metabolic pathways critical for PDAC progression (42). Fructose is common in natural foods and is also widely used in processed foods (25). Excessive fructose intake not only leads to metabolic syndrome, but also promotes the occurrence and progression of multiple tumors (8, 17, 27, 29, 31–34, 43, 44). However, the mechanism remains elusive. The present study confirms that fructose is a key nutrient that can be absorbed and metabolized by pancreatic cancer cells, thereby promoting the progression of PDAC. Fructose

Figure 6.

Fructose regulates the AMPK–mTORC1 signaling pathway in PDAC cells. **A,** Gene set enrichment analysis identified up- or downregulated pathways in tissues with high Glut5 mRNA expression based on the PDAC data from GSE15471 and GSE 28735. **B,** Western blot analysis of p70S6K expression and phosphorylation in SW1990 and BxPC3 cells cultured under different conditions at different time points. **C,** The expression of p70S6K and its phosphorylation levels in SW1990 and BxPC3 cells cultured for 12 hours in sugar-free medium containing different concentrations of fructose. **D,** The expression of p70S6K and its phosphorylation levels in Glut5-overexpressing and control cells cultured under different conditions at 2 and 12 hours. **E,** Western blot analysis of total and phosphorylated levels of AKT, ERK, and AMPK in SW1990 and BxPC3 cells cultured in different media. **F,** Western blot analysis of the effect of AMPK inhibitor Compound C (10 μmol/L) on the phosphorylation of p70S6K and AMPK in SW1990 and BxPC3 cells cultured in sugar-free medium for 24 hours. **G,** Western blot analysis of the effect of AMPK activator phenformin (10 μmol/L) on the phosphorylation of p70S6K and AMPK in SW1990 and BxPC3 cells cultured in fructose medium for 24 hours. **H,** Western blot analysis of total and phosphorylated levels of p70S6K and AMPK in SW1990 and BxPC3 cells after 24 hours of incubation in different media under hypoxia. **I,** Western blot analysis of total and phosphorylated levels of p70S6K and AMPK in Glut5-overexpressing and control cells cultured in different conditions under hypoxia for 24 hours. **J,** IHC analysis (×40) of p70S6K and AMPK phosphorylation in subcutaneous tumor tissues of three groups (control group, fructose-fed group, and glucose-fed group). **K,** The effect of AMPK activator, phenformin (10 μmol/L), and mTOR inhibitor RAD001 (3 nmol/L) on the viability of SW1990 and BxPC3 cells cultured in fructose medium for 48 hours. **L,** The effect of phenformin (10 μmol/L) and RAD001 (3 nmol/L) on the migratory ability of SW1990 and BxPC3 cells cultured in fructose medium. All data are shown as mean ± SD. Analysis was performed using one-way ANOVA followed by a Tukey test (**K** and **L**); ns, nonsignificant; **, $P < 0.01$; $n = 5$.

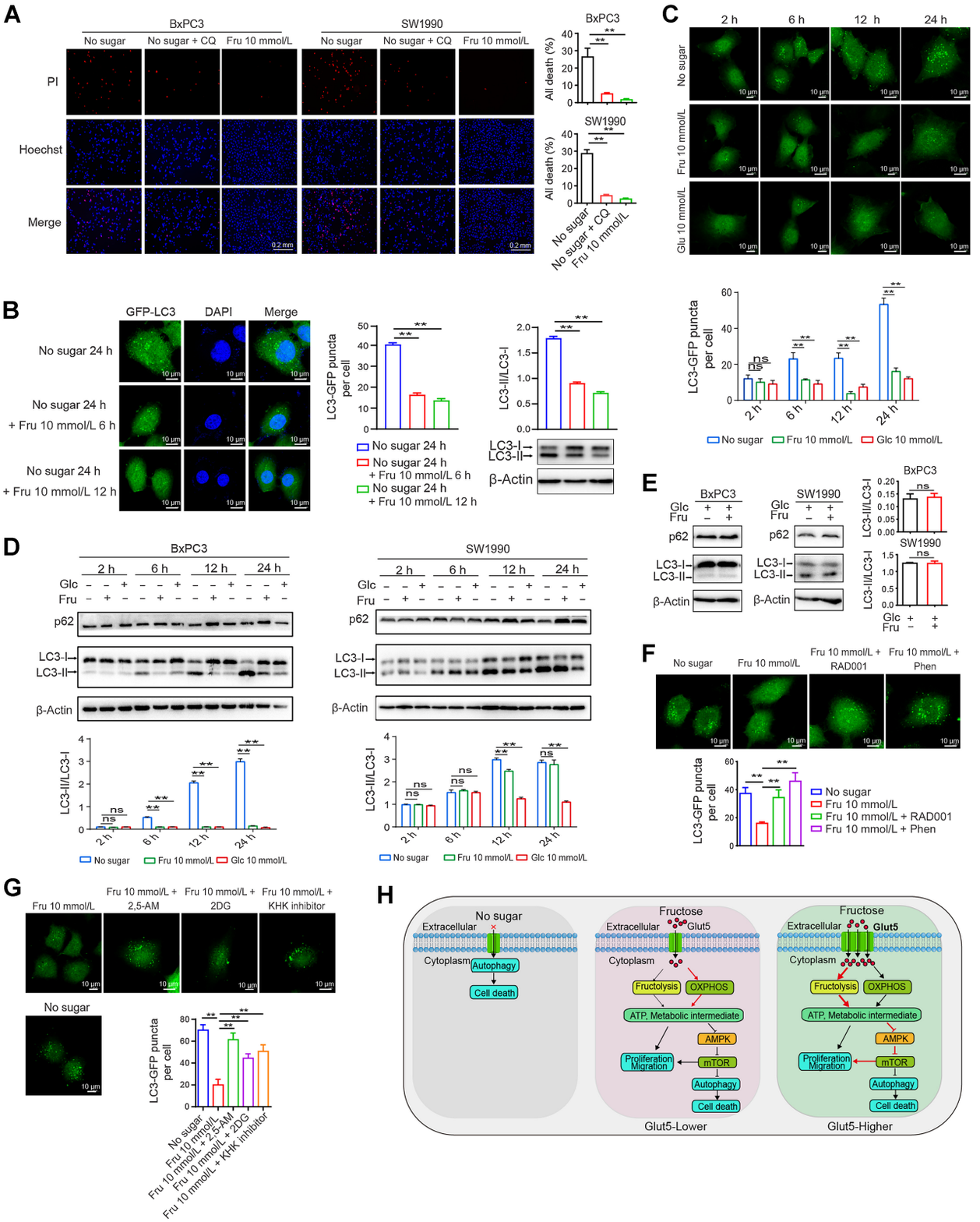
A
BxPC3
SW1990
No sugar
No sugar + CQ
Fru 10 mmol/L
PI
Hoechst
Merge
All death (%)
B
GFP-LC3
DAPI
Merge
No sugar 24 h
No sugar 24 h + Fru 10 mmol/L 6 h
No sugar 24 h + Fru 10 mmol/L 12 h
LC3-GFP puncta per cell
LC3-II/LC3-I
LC3-I
LC3-II
β-Actin
C
2 h
6 h
12 h
24 h
Glu 10 mmol/L
Glc 10 mmol/L
D
Glc
Fru
p62
E
F
Fru 10 mmol/L + RAD001
Fru 10 mmol/L + Phen
G
Fru 10 mmol/L + 2,5-AM
Fru 10 mmol/L + 2DG
Fru 10 mmol/L + KHK inhibitor
H
Fructose
Extracellular
Glut5
Cytoplasm
Autophagy
Cell death
Fructolysis
OXPHOS
ATP, Metabolic intermediate
AMPK
mTOR
Proliferation Migration
Glut5-Lower
Glut5-Higher

metabolism provides an adaptive survival mechanism for PDAC cells, especially in the presence of glucose deficiency in the tumor microenvironment. As illustrated in **Fig. 7H**, fructose not only inhibits cellular hyperautophagy and subsequent cell death due to glucose deficiency by regulating the AMPK–mTORC1 signaling pathway, but also promotes tumor progression by providing ATP and available carbon sources to tumor cells. Moreover, fructose intake by PDAC cells can influence the metabolic phenotype of the cells, making them more adaptable to the tumor microenvironment. In addition, the fructose-transporter Glut5 is highly expressed in PDAC tissues and serves as an independent prognostic marker in patients with PDAC. Therefore, targeting fructose metabolism may be a potential therapeutic strategy for PDAC.

Our findings support the notion that Glut5-mediated fructose uptake and utilization confers PDAC progression. Although previous studies have linked increased fructose intake to the initiation and aggressiveness of several malignancies, including pancreatic cancer; however, a systematic analysis of fructose metabolism on the progression of this lethal disease is still lacking (34). In this study, both our IHC results and database analysis of HPA and TCGA showed that Glut5 expression was significantly higher in PDAC tissues than in normal tissues, suggesting that increased fructose intake may be involved in the development of PDAC. Given the poor vascularization in PDAC tissues, cancer cells must remodel their metabolism to adapt to the severe nutrient limitations, such as glucose-deficient tumor microenvironment. Thus, elevated Glut5 allows cancer cells to use fructose to compensate for glucose shortage. Consistent with this speculation, fructose was effective in maintaining the survival and proliferation of PDAC cells in the absence of glucose, and this effect was more pronounced in Glut5-overexpressing cells. In addition, inhibition of Glut5 or blocking fructose catabolism with inhibitors inhibited the pro-survival and proliferative effects of fructose, further demonstrating the pro-growth role of fructose in pancreatic cancer. Moreover, in both types of murine allograft models, fructose even exhibited stronger tumor growth-promoting effects than glucose. Consistently, tumor tissues from mice with high fructose intake had the highest proliferation index and the lowest apoptosis rate. Thus, fructose plays a stronger role than glucose in accelerating tumor growth *in vivo*. These data also suggest that fructose is not only a substitute for glucose, but may play a different role. Interestingly, in both types of PDAC metastasis models, high-fructose feeding significantly promoted the metastasis of pancreatic cancer cells in mice, especially in the lung metastasis model. Similarly, fructose also enhanced the migration and invasion abilities of PDAC cells *in vitro*. Consistently, a previous study using a different model also demonstrated that high fructose promotes the metastatic potential of advanced pancreatic cancer (45). In line with these observations, clinical evidence, including our data and the TCGA database, indicates that patients with PDAC with high Glut5 expression have a worse prognosis and that Glut5 levels are an independent prognostic marker for patients with PDAC. Together, fructose not only maintains cancer cell survival and proliferation, but also promotes PDAC progression.

How PDAC cells use and metabolize fructose is worth investigating. Because fructose has the same molecular formula as glucose, it is traditionally believed that the metabolic processes of both are similar (34). However, recent studies have shown that fructose is not a simple substitute for glucose, and that the two are metabolized quite differently in cancer cells, with different effects on the malignant behavior of tumors. For instance, in lung and intestinal tumors, fructose can promote tumor growth by increasing fatty acids synthesis (8, 17). Leukemic cells can adapt to a low-glucose microenvironment by relying on the fructose-upregulated serine synthesis pathway to produce large amounts of alpha-ketoglutarate to replenish the TCA cycle (46). These findings suggest that different types of tumors have their own preferences in the way they use and metabolize fructose. Our present study strongly suggests that fructose may regulate the overall metabolic composition of PDAC cells. Consistently, fructose metabolites such as D-6-phosphofructose and D-1-phosphofructose were significantly upregulated in fructose group cells. Thus, fructose intake may lead to a reprogramming of the metabolic profile of PDAC cells. In addition, fructose intake enhanced the metabolism of the galactose pathway, amino, and nucleotide sugars, suggesting that fructose may promote the level of protein glycosylation in PDAC cells. Because fructose is 8–10 times more reactive than glucose in promoting glycosylation and also plays a more important role in the formation of advanced glycosylation end products (47), these results suggest that in addition to providing an essential carbon source for tumor cell growth, fructose may also influence cancer cell function by regulating the overall level of protein glycosylation. Furthermore, it remains to be determined whether fructose can up- or downregulate intracellular ATP levels, as there are conflicting reports (37, 48, 49). Notably, fructose did not alter intracellular ATP levels under glucose-rich conditions, but upregulated ATP levels under glucose-deficient conditions. We hypothesize that this may be due to the fact that intracellular ATP levels have reached a maximum under sugar-sufficient conditions, and that although fructose metabolism produces ATP, it does not alter the maximum level of ATP. Interestingly, PDAC cells with low Glut5 expression metabolized fructose mainly through OXPHOS to produce ATP, whereas cells with high Glut5 expression metabolized fructose to produce ATP mainly through glycolysis. Consistently, analysis of the TCGA database showed that the expression level of Glut5 was positively correlated with the glycolysis-related gene set and negatively correlated with the OXPHOS gene set. Thus, high expression of Glut5 leads to a reprogramming of fructose metabolism in favor of the glycolytic pathway. In line with these evidences, upregulation of Glut5 promotes cholangiocarcinoma progression by enhancing glycolysis and

Figure 7.

Fructose reduces sugar-free–induced cell death by inhibiting autophagy. **A,** Effect of chloroquine (CQ; 50 μmol/L) and fructose on the death of SW1990 and BxPC3 cells after 48 hours of sugar starvation. Cell nuclei were visualized with Hoechst. Dead cells were stained with PI. **B,** BxPC3 cells were transfected with GFP–LC3 plasmid, and the effect of fructose on GFP–LC3 puncta and LC3-I/II expression levels of BxPC3/GFP–LC3 cells was detected after 24 hours of sugar starvation. Images were taken using a confocal microscope. **C,** GFP-LC3 puncta of BxPC3/ GFP–LC3 cells at different time points under the indicated culture conditions. **D,** LC3-I/II and P62 expression levels of BxPC3 and SW1990 cells at different time points under different culture conditions as described in **D**. **E,** Effect of fructose on the LC3II/I ratio and p62 protein expression under glucose sufficiency conditions. **F,** GFP–LC3 puncta of BxPC3/GFP–LC3 cells under sugar starvation or fructose treatment in the presence of phenformin (10 μmol/L) or RAD001 (3 nmol/L) for 24 hours. **G,** GFP–LC3 puncta of BxPC3/GFP-LC3 cells under sugar starvation or fructose treatment in the presence of 2, 5-AM (3 mmol/L), 2-DG (2 mmol/L), or KHK inhibitor (1 μmol/L) for 24 hours. **H,** Schematic diagram of the effect of fructose and Glut5 overexpression on the functions of PDAC cells. All data are shown as mean ± SD. Analysis was performed using an unpaired Student *t* test (**E**) or one-way ANOVA followed by a Tukey test (**A**, **B**, **F**, and **G**) or two-way ANOVA followed by a Tukey test (**C** and **D**); ns, nonsignificant; **, $P < 0.01$; $n = 3$.

ATP production (43). Collectively, these results suggest that fructose metabolism is critical to drive PDAC progression, especially in the presence of glucose deficiency.

Another key finding of this study is that fructose maintains the survival and proliferation of PDAC cells by inhibiting autophagy. Autophagy, as an adaptive cellular behavior, plays an important role in responding to environmental stress and maintaining cell survival (39). However, if these stress persist, excessive autophagy can lead to programmed cell death (50). This study found that chloroquine inhibited sugar deprivation–induced cell death and that this death could also be reversed by the addition of fructose, suggesting that fructose maintains cell survival by inhibiting autophagy induced by sugar deprivation. The mechanism by which fructose inhibits autophagy is very intriguing. Considering that autophagy is usually triggered by nutrient and energy deficiencies, and fructose metabolism can provide cells with ATP and carbon sources. In addition, the AMPK/mTORC1 signaling is a key intracellular energy sensor pathway and is also associated with autophagic degradation in eukaryotes (51). Therefore, it is reasonable to assume that fructose inhibits autophagy by regulating the AMPK/mTORC1 pathway. As expected, fructose significantly inhibited AMPK activation and activated mTORC1 signaling under glucose-free conditions. Likewise, a recent study on lung cancer also found that fructose can lead to activation of mTORC1 by inhibiting AMPK (17). Notably, fructose did not alter the activation of AKT and ERK (the main upstream activators of mTORC1), suggesting that fructose-induced activation of mTORC1 is mainly achieved by inhibiting AMPK activity. Consistently, the AMPK inhibitor Com. C upregulated the activation of p70S6K (a downstream kinase of mTORC1) in sugar-free medium in PDAC cells, whereas the AMPK activator Phen inhibited the activation of p70S6K in fructose medium. Moreover, the mTORC1 inhibitor RAD001 and the AMPK activator Phen significantly prevented the autophagy-inhibiting effect of fructose and also inhibited the proliferation and migration abilities of PDAC cells cultured in fructose medium. Furthermore, inhibition of fructose metabolism in fructose medium resulted in a significant increase in autophagy in PDAC cells. Collectively, these findings illustrated a crucial role of fructose in inhibiting sugar deprivation–induced autophagic cell death by regulating the AMPK–mTORC1 signaling pathway.

In conclusion, our data suggest that Glut5-mediated fructose uptake and utilization confer PDAC progression when glucose is deficient. Fructose is not a simple alternative fuel to glucose; in addition to providing ATP production and a carbon source, fructose modulates key intracellular signaling pathways and metabolic plasticity. We provide evidence that the fructose-regulated AMPK–mTORC1 signaling pathway inhibits autophagy-induced cell death, making pancreatic cancer cells more conducive to growth and progression. From a therapeutic perspective, the Glut5–AMPK/mTORC1 signaling pathway may be a potential target for the treatment of PDAC. Therefore, an in-depth investigation of the relationship between fructose consumption and pancreatic cancer is crucial, as dietary intake is highly modifiable and dietary changes may represent an opportunity for primary cancer prevention.

Authors' Disclosures

No disclosures were reported.

Authors' Contributions

Y. Cui: Conceptualization, resources, data curation, investigation, project administration. **J. Tian:** Data curation, methodology. **Z. Wang:** Software, investigation. **H. Guo:** Methodology. **H. Zhang:** Software, validation. **Z. Wang:** Supervision, visualization. **H. Liu:** Formal analysis, methodology. **W. Song:** Software, validation. **L. Liu:** Resources, formal analysis. **R. Tian:** Methodology. **X. Zuo:** Software. **S. Ren:** Data curation. **R. Niu:** Conceptualization, funding acquisition, project administration. **F. Zhang:** Conceptualization, resources, data curation, writing–original draft, project administration, writing–review and editing.

Acknowledgments

This research was supported by grants from the National Natural Science Foundation of China (numbers 82073085, 82073252, and 81772804), Tianjin Municipal Science and Technology Commission (number 20JCZDJC00030), and Changjiang Scholars and Innovative Research Team (number IRT_14R40).

The publication costs of this article were defrayed in part by the payment of publication fees. Therefore, and solely to indicate this fact, this article is hereby marked "advertisement" in accordance with 18 USC section 1734.

Note

Supplementary data for this article are available at Cancer Research Online (http://cancerres.aacrjournals.org/).

Received February 14, 2023; revised August 2, 2023; accepted September 19, 2023; published first September 22, 2023.

References

1. Kleeff J, Korc M, Apte M, La Vecchia C, Johnson CD, Biankin AV, et al. Pancreatic cancer. Nat Rev Dis Primers 2016;2:16022.
2. Wood LD, Canto MI, Jaffee EM, Simeone DM. Pancreatic cancer: pathogenesis, screening, diagnosis, and treatment. Gastroenterology 2022;163:386–402.
3. Paternoster S, Falasca M. The intricate relationship between diabetes, obesity, and pancreatic cancer. Biochim Biophys Acta Rev Cancer 2020; 1873:188326.
4. Kirkegard J, Mortensen FV, Cronin-Fenton D. Chronic pancreatitis and pancreatic cancer risk: a systematic review and meta-analysis. Am J Gastroenterol 2017;112:1366–72.
5. Connor AA, Gallinger S. Pancreatic cancer evolution and heterogeneity: integrating omics and clinical data. Nat Rev Cancer 2022;22:131–42.
6. Ebert K, Witt H. Fructose malabsorption. Mol Cell Pediatr 2016;3:10.
7. Hannou SA, Haslam DE, McKeown NM, Herman MA. Fructose metabolism and metabolic disease. J Clin Invest 2018;128:545–55.
8. Goncalves MD, Lu C, Tutnauer J, Hartman TE, Hwang SK, Murphy CJ, et al. High-fructose corn syrup enhances intestinal tumor growth in mice. Science 2019;363:1345–9.
9. Carreno D, Corro N, Torres-Estay V, Veliz LP, Jaimovich R, Cisternas P, et al. Fructose and prostate cancer: toward an integrated view of cancer cell metabolism. Prostate Cancer Prostatic Dis 2019;22:49–58.
10. Gao W, Li N, Li Z, Xu J, Su C. Ketohexokinase is involved in fructose utilization and promotes tumor progression in glioma. Biochem Biophys Res Commun 2018;503:1298–306.
11. Bu P, Chen KY, Xiang K, Johnson C, Crown SB, Rakhilin N, et al. Aldolase B-mediated fructose metabolism drives metabolic reprogramming of colon cancer liver metastasis. Cell Metab 2018;27:1249–62.
12. Fan X, Liu H, Liu M, Wang Y, Qiu L, Cui Y. Increased utilization of fructose has a positive effect on the development of breast cancer. PeerJ 2017;5:e3804.
13. Chen WL, Wang YY, Zhao A, Xia L, Xie G, Su M, et al. Enhanced fructose utilization mediated by SLC2A5 is a unique metabolic feature of acute myeloid leukemia with therapeutic potential. Cancer Cell 2016;30:779–91.
14. Charrez B, Qiao L, Hebbard L. The role of fructose in metabolism and cancer. Horm Mol Biol Clin Investig 2015;22:79–89.
15. Port AM, Ruth MR, Istfan NW. Fructose consumption and cancer: is there a connection? Curr Opin Endocrinol Diabetes Obes 2012;19:367–74.

16. Monzavi-Karbassi B, Hine RJ, Stanley JS, Ramani VP, Carcel-Trullols J, Whitehead TL, et al. Fructose as a carbon source induces an aggressive phenotype in MDA-MB-468 breast tumor cells. Int J Oncol 2010;37: 615–22.
17. Chen WL, Jin X, Wang M, Liu D, Luo Q, Tian H, et al. GLUT5-mediated fructose utilization drives lung cancer growth by stimulating fatty acid synthesis and AMPK/mTORC1 signaling. Jci Insight 2020;5:e131596.
18. Strober JW, Brady MJ. Dietary fructose consumption and triple-negative breast cancer incidence. Front Endocrinol 2019;10:367.
19. Romieu I, Lazcano-Ponce E, Sanchez-Zamorano LM, Willett W, Hernandez-Avila M. Carbohydrates and the risk of breast cancer among Mexican women. Cancer Epidemiol Biomarkers Prev 2004;13:1283–9.
20. Aune D, Chan DSM, Vieira AR, Navarro Rosenblatt DA, Vieira R, Greenwood DC, et al. Dietary fructose, carbohydrates, glycemic indices and pancreatic cancer risk: a systematic review and meta-analysis of cohort studies. Ann Oncol 2012;23:2536–46.
21. Liu H, Heaney AP. Refined fructose and cancer. Expert Opin Ther Targets 2011; 15:1049–59.
22. Taylor SR, Ramsamooj S, Liang RJ, Katti A, Pozovskiy R, Vasan N, et al. Dietary fructose improves intestinal cell survival and nutrient absorption. Nature 2021; 597:263–7.
23. Nakagawa T, Lanaspa MA, Millan IS, Fini M, Rivard CJ, Sanchez-Lozada LG, et al. Fructose contributes to the Warburg effect for cancer growth. Cancer Metab 2020;8:16.
24. Herman MA, Birnbaum MJ. Molecular aspects of fructose metabolism and metabolic disease. Cell Metab 2021;33:2329–54.
25. Shi YN, Liu YJ, Xie Z, Zhang WJ. Fructose and metabolic diseases: too much to be good. Chin Med J 2021;134:1276–85.
26. Medina Villaamil V, Aparicio Gallego G, Valbuena Rubira L, Garcia Campelo R, Valladares-Ayerbes M, Grande Pulido E, et al. Fructose-transporter GLUT5 expression in clear renal cell carcinoma. Oncol Rep 2011;25:315–23.
27. Jin C, Gong X, Shang Y. GLUT5 increases fructose utilization in ovarian cancer. Onco Targets Ther 2019;12:5425–36.
28. Zhou X, Qin X, Gong T, Zhang ZR, Fu Y. d-Fructose modification enhanced internalization of mixed micelles in breast cancer cells via GLUT5 transporters. Macromol Biosci 2017;17:1600529.
29. Su C, Li H, Gao W. GLUT5 increases fructose utilization and promotes tumor progression in glioma. Biochem Biophys Res Commun 2018;500:462–9.
30. Zamora-Leon SP, Golde DW, Concha II, Rivas CI, Delgado-Lopez F, Baselga J, et al. Expression of the fructose-transporter GLUT5 in human breast cancer. Proc Natl Acad Sci USA 1996;93:1847–52.
31. Wlodarczyk J, Wlodarczyk M, Zielinska M, Jedrzejczak B, Dziki L, Fichna J. Blockade of fructose-transporter protein GLUT5 inhibits proliferation of colon cancer cells: proof of concept for a new class of antitumor therapeutics. Pharmacol Rep 2021;73:939–45.
32. Shen Z, Li Z, Liu Y, Li Y, Feng X, Zhan Y, et al. GLUT5–KHK axis-mediated fructose metabolism drives proliferation and chemotherapy resistance of colorectal cancer. Cancer Lett 2022;534:215617.
33. Yang J, Dong C, Wu J, Liu D, Luo Q, Jin X. Fructose utilization enhanced by GLUT5 promotes lung cancer cell migration via activating glycolysis/AKT pathway. Clin Transl Oncol 2022;25:1080–90.
34. Liu H, Huang D, McArthur DL, Boros LG, Nissen N, Heaney AP. Fructose induces transketolase flux to promote pancreatic cancer growth. Cancer Res 2010;70:6368–76.
35. Gao Z, Han X, Zhu Y, Zhang H, Tian R, Wang Z, et al. Drug-resistant cancer cell-derived exosomal EphA2 promotes breast cancer metastasis via the EphA2–Ephrin A1 reverse signaling. Cell Death Dis 2021;12:414.
36. Han B, Zhang H, Tian R, Liu H, Wang Z, Wang Z, et al. Exosomal EPHA2 derived from highly metastatic breast cancer cells promotes angiogenesis by activating the AMPK signaling pathway through Ephrin A1-EPHA2 forward signaling. Theranostics 2022;12:4127–46.
37. Jiang H, Lin Q, Ma L, Luo S, Jiang X, Fang J, et al. Fructose and fructose kinase in cancer and other pathologies. J Genet Genomics 2021;48:531–9.
38. Hou J, Li X, Xie KP. Coupled liquid biopsy and bioinformatics for pancreatic cancer early detection and precision prognostication. Mol Cancer 2021;20:34.
39. Miller DR, Thorburn A. Autophagy and organelle homeostasis in cancer. Dev Cell 2021;56:906–18.
40. Martinez-Reyes I, Chandel NS. Cancer metabolism: looking forward. Nat Rev Cancer 2021;21:669–80.
41. Sun L, Zhang H, Gao P. Metabolic reprogramming and epigenetic modifications on the path to cancer. Protein Cell 2022;13:877–919.
42. Encarnacion-Rosado J, Kimmelman AC. Harnessing metabolic dependencies in pancreatic cancers. Nat Rev Gastroenterol Hepatol 2021;18:482–92.
43. Suwannakul N, Armartmuntree N, Thanan R, Midorikawa K, Kon T, Oikawa S, et al. Targeting fructose metabolism by glucose-transporter 5 regulation in human cholangiocarcinoma. Genes Dis 2022;9:1727–41.
44. Weng Y, Zhu J, Chen Z, Fu J, Zhang F. Fructose fuels lung adenocarcinoma through GLUT5. Cell Death Dis 2018;9:557.
45. Hsieh CC, Shyr YM, Liao WY, Chen TH, Wang SE, Lu PC, et al. Elevation of beta-galactoside alpha2,6-sialyltransferase 1 in a fructoseresponsive manner promotes pancreatic cancer metastasis. Oncotarget 2017;8:7691–709.
46. Jeong S, Savino AM, Chirayil R, Barin E, Cheng Y, Park SM, et al. High fructose drives the serine synthesis pathway in acute myeloid leukemic cells. Cell Metab 2021;33:145–59.
47. Gugliucci A. Formation of fructose-mediated advanced glycation end products and their roles in metabolic and inflammatory diseases. Adv Nutr 2017;8:54–62.
48. Latta M, Kunstle G, Leist M, Wendel A. Metabolic depletion of ATP by fructose inversely controls CD95^{-} and tumor necrosis factor receptor 1-mediated hepatic apoptosis. J Exp Med 2000;191:1975–85.
49. Wu KL, Hung CY, Chan JY, Wu CW. An increase in adenosine-5'-triphosphate (ATP) content in rostral ventrolateral medulla is engaged in the high fructose diet-induced hypertension. J Biomed Sci 2014;21:8.
50. Noguchi M, Hirata N, Tanaka T, Suizu F, Nakajima H, Chiorini JA. Autophagy as a modulator of cell death machinery. Cell Death Dis 2020;11:517.
51. Lin SC, Hardie DG. AMPK: sensing glucose as well as cellular energy status. Cell Metab 2018;27:299–313.